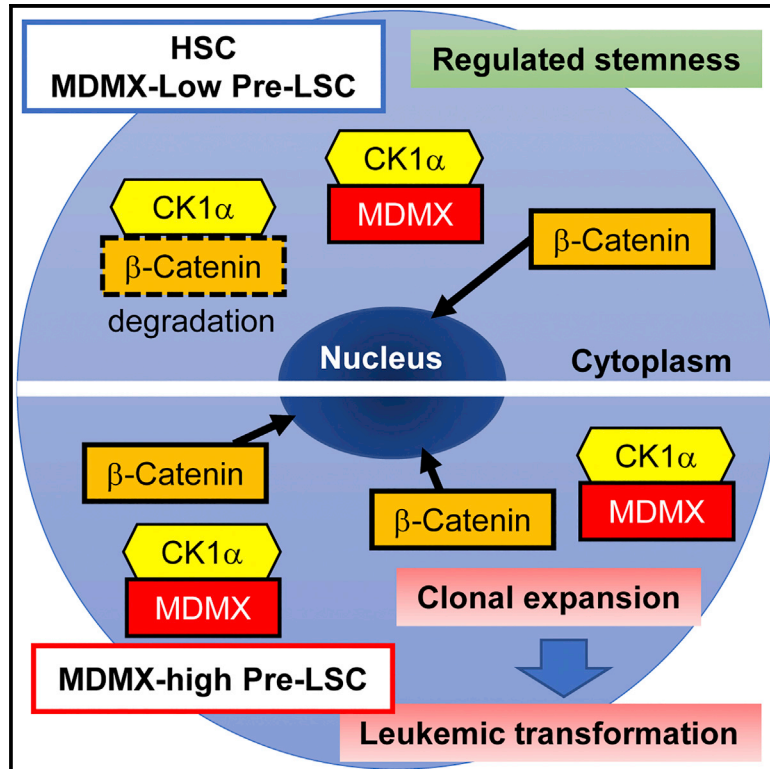


MDMX acts as a pervasive preleukemic-to-acute myeloid leukemia transition mechanism

Graphical abstract



Authors

Koki Ueda, Rajni Kumari, Emily Schwenger, ..., Jacqueline Boultonwood, Amit Verma, Ulrich Steidl

Correspondence

ulrich.steidl@einsteinmed.org

In brief

Using mouse models and data from MDS patients, Ueda et al. identify MDMX as a pervasive preleukemic-to-acute myeloid leukemia transition mechanism across multiple different genetic disease subtypes. MDMX physically interacts with CK1 α , inducing accumulation of β -Catenin. Blocking both canonical and non-canonical activity of MDMX enhances therapeutic effects against preleukemia/leukemia.

Highlights

- MDMX overexpression induces preleukemic-to-AML transition in multiple mouse models
- MDMX causes preleukemic-to-AML transition by p53-independent activation of β -Catenin
- MDMX binds to CK1 α and prevents CK1 α -dependent degradation of β -Catenin
- MDMX overexpression correlates with progression to AML in patients with MDS



Article

MDMX acts as a pervasive preleukemic-to-acute myeloid leukemia transition mechanism

Koki Ueda,¹ Rajni Kumari,^{1,11} Emily Schwenger,^{1,11} Justin C. Wheat,¹ Oliver Bohorquez,¹ Swathi-Rao Narayanagari,^{1,2,3} Samuel J. Taylor,¹ Luis A. Carvajal,¹ Kith Pradhan,⁴ Boris Bartholdy,¹ Tihomira I. Todorova,¹ Hiroki Goto,¹ Daqian Sun,^{1,2,3} Jiahao Chen,¹ Jidong Shan,⁵ Yinghui Song,⁵ Cristina Montagna,⁵ Shunbin Xiong,⁶ Guillermina Lozano,⁶ Andrea Pellagatti,⁷ Jacqueline Boulwood,⁷ Amit Verma,^{2,8,9,10} and Ulrich Steidl^{1,2,8,9,10,12,*}

¹Department of Cell Biology, Albert Einstein College of Medicine, Bronx, NY 10461, USA

²Ruth L. and David S. Gottesman Institute for Stem Cell Research and Regenerative Medicine, Albert Einstein College of Medicine, Bronx, NY 10461, USA

³Stem Cell Isolation and Xenotransplantation Facility, Albert Einstein College of Medicine, Bronx, NY 10461, USA

⁴Department of Epidemiology & Population Health, Albert Einstein College of Medicine, Bronx, NY 10461, USA

⁵Department of Genetics, Albert Einstein College of Medicine, Bronx, NY 10461, USA

⁶Department of Genetics, Division of Basic Science Research, The University of Texas, MD Anderson Cancer Center, Houston, TX 77030, USA

⁷Blood Cancer UK Molecular Haematology Unit, Nuffield Division of Clinical Laboratory Sciences, Radcliffe Department of Medicine, and NIHR Oxford Biomedical Research Centre, University of Oxford, Oxford OX3 9DU, UK

⁸Division of Hemato-Oncology, Department of Medicine (Oncology), Albert Einstein College of Medicine – Montefiore Medical Center, Bronx, NY 10461, USA

⁹Blood Cancer Institute, Albert Einstein College of Medicine – Montefiore Medical Center, Bronx, NY 10461, USA

¹⁰Albert Einstein Cancer Center, Albert Einstein College of Medicine – Montefiore Medical Center, Bronx, NY 10461, USA

¹¹These authors contributed equally

¹²Lead contact

*Correspondence: ulrich.steidl@einsteinmed.org

<https://doi.org/10.1016/j.ccell.2021.02.006>

SUMMARY

MDMX is overexpressed in the vast majority of patients with acute myeloid leukemia (AML). We report that MDMX overexpression increases preleukemic stem cell (pre-LSC) number and competitive advantage. Utilizing five newly generated murine models, we found that MDMX overexpression triggers progression of multiple chronic/asymptomatic preleukemic conditions to overt AML. Transcriptomic and proteomic studies revealed that MDMX overexpression exerts this function, unexpectedly, through activation of Wnt/ β -Catenin signaling in pre-LSCs. Mechanistically, MDMX binds CK1 α and leads to accumulation of β -Catenin in a p53-independent manner. Wnt/ β -Catenin inhibitors reverse MDMX-induced pre-LSC properties, and synergize with MDMX-p53 inhibitors. Wnt/ β -Catenin signaling correlates with MDMX expression in patients with preleukemic myelodysplastic syndromes and is associated with increased risk of progression to AML. Our work identifies MDMX overexpression as a pervasive preleukemic-to-AML transition mechanism in different genetically driven disease subtypes, and reveals Wnt/ β -Catenin as a non-canonical MDMX-driven pathway with therapeutic potential for progression prevention and cancer interception.

INTRODUCTION

While mutations in the tumor suppressor p53 (Tumor Protein P53 [TP53]) are very common in various solid tumors (Kandoth et al., 2013; Muller and Vousden, 2013), they are relatively rare (<10% of patients) in patients with acute myeloid leukemia (AML) (Fenaux et al., 1992; Kadia et al., 2016; Peller and Rotter, 2003; Zeisig et al., 2012). In the majority of AML with wild-type (WT) TP53, p53 protein function is inhibited by its suppressors, Murine Double Minute 2 (MDM2) and Murine Double Minute X (MDMX, also known as MDM4) (Wade et al., 2013). In particular, MDMX, which interacts with p53 and prevents its transactivation, is overexpressed in

the vast majority of patients with AML (~90%), including at the stem cell level, in part due to altered splicing between a short form and more stable full-length MDMX transcript (Carvajal et al., 2018; Han et al., 2016).

We and others have previously demonstrated that AML with WT TP53 is responsive to a novel MDMX/MDM2 dual inhibitor (ALRN-6924), and several clinical trials are currently ongoing (Carvajal et al., 2018; Sallman et al., 2018). However, the precise contribution and causative effects of MDMX overexpression and its functional consequences on normal and malignant hematopoiesis have not yet been studied. This is of particular significance for preleukemic aberrations and conditions. While AML



is characterized by substantial genetic and epigenetic inter-patient as well as intra-patient subclonal heterogeneity (Cancer Genome Atlas Research Network et al., 2013; Li et al., 2016; Paemmanuil et al., 2016), a large body of recent work has established preleukemic stem cells (pre-LSCs) as the initial reservoir for consecutive transformation to overt leukemia (Bereshchenko et al., 2009; Busque et al., 2012; Chen et al., 2019; Genovese et al., 2014; Jaiswal et al., 2014; Jan et al., 2012; Kuo et al., 2006; Shlush et al., 2014, 2017; Steidl et al., 2006; Will et al., 2012, 2015; Xie et al., 2014). However, despite increasing investigation and more refined characterization of pre-LSCs, the mechanisms that trigger the preleukemic to overt leukemic transition (i.e., that are causative for genetically aberrant pre-LSC to progress to AML rather than remaining compatible with healthy aging in the vast majority of individuals) remain largely unclear. This prompted us to systematically study MDMX overexpression in the context of different, frequently occurring preleukemic aberrations to assess its possible role as a pervasive preleukemic-to-AML transition mechanism.

RESULTS

MDMX overexpression increases the number, proliferation, and competitiveness of hematopoietic stem cells

To investigate the role of MDMX overexpression in normal and malignant hematopoiesis, we utilized *Mdmx* transgenic mice (*Mdmx*-Tg), which die from a variety of solid tumors or lymphomas after long latency (median of 550 days), without evidence of any myeloid lineage disorders (Xiong et al., 2010, 2017).

First, we analyzed hematological phenotypes of *Mdmx*-Tg compared with WT littermates. Hematopoietic stem and progenitor cells (HSPCs; lineage⁻ cKit⁺) from *Mdmx*-Tg animals overexpressed *Mdmx* 2.9 ± 0.1 fold on average compared with WT. *Mdmx* expression in hematopoietic stem cells (HSCs; lineage⁻ cKit⁺ Sca-1⁺(LSK) Flk2⁻) was 17.3-fold ± 7.4-fold elevated compared with WT (Figure S1A, left and center). Also, we measured the ratio of oncogenic full-length *Mdmx* (*Mdmx*-FL) against short-form *Mdmx* (*Mdmx*-S; reported to suppress oncogenic activity of MDMX-FL) as previously described (Dewaele et al., 2016). The Percent Spliced In (PSI) index (*Mdmx*-FL/*Mdmx*-FL+*Mdmx*-S) was approximately 0.6 in WT HSCs, and nearly 1 in *Mdmx*-Tg HSCs, suggesting that relative levels of endogenous *Mdmx*-S are minimal in transgenic mice (Figure S1A, right). Blood cell counts were similar between *Mdmx*-Tg and WT throughout the life span, suggesting that MDMX overexpression alone does not cause any overt change in hematopoiesis (Figure S1B). Total bone marrow (BM) cell count of 3-month-old *Mdmx*-Tg mice was also similar to WT controls (Figure S1C). We analyzed BM HSPCs by flow cytometry (FCM), and detected no significant differences in *Mdmx*-Tg compared with WT controls in the number of progenitors or LSK cells (Figure S1D). Also, spleen weight and cellularity in 3-month-old *Mdmx*-Tg mice were indistinguishable from WT controls (Figures S1E and S1F). However, more detailed analysis of the BM LSK fraction revealed that phenotypic long term HSCs (LT-HSC; Flk2^{low}, CD48^{low}, CD150^{high} LSK) were increased in *Mdmx*-Tg compared with WT mice (Figure 1A). We compared cell cycling of HSCs (Flk2⁻ LSK) by *in vivo* BrdU assays of

Mdmx-Tg compared with WT littermates. BrdU uptake in *Mdmx*-Tg HSCs was significantly increased, indicative of faster proliferation of HSCs (Figure 1B). In addition, *Mdmx*-Tg BM cells displayed significantly increased serial replating capacity in methylcellulose relative to WT BM cells (Figure 1C).

To determine whether HSCs from *Mdmx*-Tg animals have increased functional repopulating capacity compared with WT controls *in vivo*, we performed competitive congenic transplantation experiments. While homing of Ly45.2⁺ WT and *Mdmx*-Tg cells to the BM right after transplantation was indistinguishable (Figure S1G), *Mdmx*-Tg cells significantly outcompeted WT cells over time, and in both the myeloid and lymphoid lineages (Figure 1D). Collectively, our data reveal that HSCs in *Mdmx*-Tg mice are increased in number, proliferative activity, *in vitro* serial replating capacity, and *in vivo* repopulating capacity, compared with HSCs from WT control mice.

MDMX overexpression acts as a preleukemic-to-AML transition mechanism in conjunction with different myeloid disease alleles

Next, we wanted to interrogate a potential cooperative effect of MDMX overexpression in the contexts of known leukemia-driving aberrations.

MDMX overexpression transforms *PU.1* knockdown-induced pre-LSC

We crossed *Mdmx*-Tg mice with *PU.1* upstream regulatory element (URE) knockout mice (URE^{-/-}), which lack a *PU.1* URE resulting in 80% reduction of expression of *PU.1* compared with WT controls and develop AML at 4 to 8 months of age (Rosenbauer et al., 2004). *PU.1* downregulation is a very frequent (50%–70%) preleukemic event in both mouse and human (Lavallee et al., 2015; Mizuki et al., 2003; Muller and Vousden, 2013; Sive et al., 2016; Steidl et al., 2006, 2007; Vangala et al., 2003; Will et al., 2015; Yoshida et al., 2007). Young URE^{-/-} mice (2 to 4 months old) display preleukemic characteristics, including at the stem cell level, and have myeloid-skewed hematopoiesis but do not give rise to overt AML upon transplantation, and can therefore be utilized as a preleukemic-to-leukemic transition model (Steidl et al., 2006). To test whether MDMX overexpression plays a role in the preleukemia-to-AML transition, we transplanted preleukemic BM cells from preleukemic 3-month-old URE^{-/-}; *Mdmx*-Tg or 4-month-old URE^{-/-}, or leukemic 4-month-old URE^{-/-}; *Mdmx*-Tg animals into sublethally irradiated NOD-SCID IL2R-gamma null (NSG) mice (Figure 2A). BM cells from 4-month-old URE^{-/-} mice, as expected, did not cause AML in recipients. However, BM cells of 4-month-old URE^{-/-}; *Mdmx*-Tg animals were sufficient to precipitate overt AML in recipients (Figure 2B). Moreover, when we performed the transplantation with younger, preleukemic URE^{-/-}; *Mdmx*-Tg BM cells at 3 months of age, we obtained the same result of induction of overt AML in all recipient animals, albeit at a slightly longer latency (Figures 2B and 2C). These findings indicate that MDMX overexpression plays a causative role in the preleukemic-to-AML transition in the context of *PU.1* inactivation. We therefore further investigated the preleukemic stage of URE^{-/-}; *Mdmx*-Tg mice. Immunophenotypic Flk2⁻ LSK cells of URE^{-/-}; *Mdmx*-Tg mice had 7.1-fold ± 1.2-fold higher *Mdmx* levels compared with URE^{-/-} Flk2⁻ LSK cells (pre-LSCs) (Figure S2A). Interestingly, 3-month-old URE^{-/-}; *Mdmx*-Tg mice

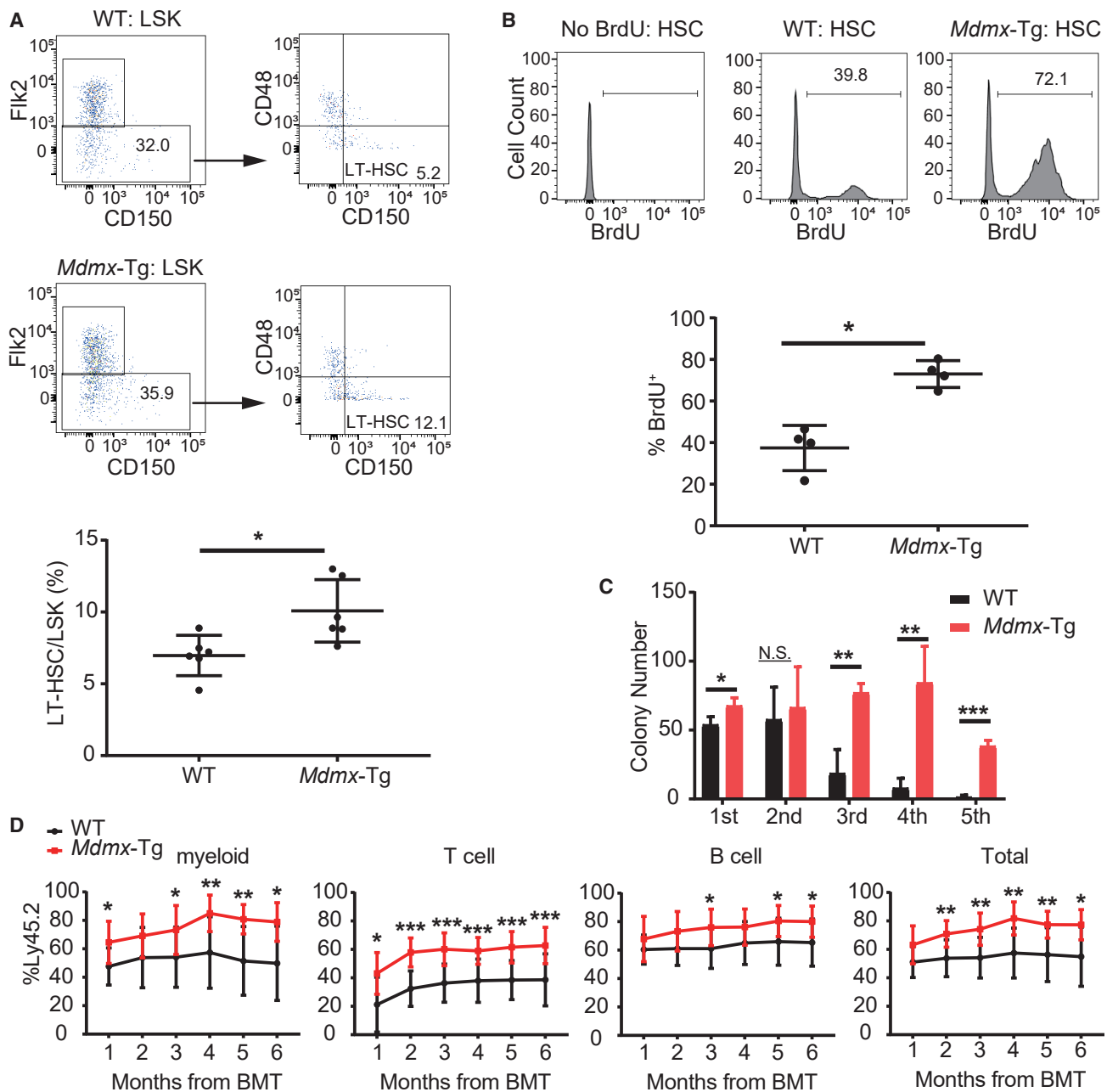


Figure 1. MDMX overexpression increases the number, proliferation, and competitiveness of HSCs

(A) Upper: representative flow cytometric plots of BM LSK cells from a 3-month-old WT and *Mdmx*-Tg mouse. Lower: ratio of Fik2^{low} CD48^{low} CD150^{high} LT-HSC in LSK (%) are shown (n = 6).
 (B) Upper: BrdU uptake in HSCs (Fik2⁻ LSK) after 48 h of treatment with 1 mg/mL BrdU in drinking water. Representative flow cytometric plots. Lower: ratio of BrdU⁺ HSCs are shown (n = 4).
 (C) Colony number from serial replating assays of 1 × 10⁴ bulk BM cells (n = 4).
 (D) 1.0 × 10⁶ WT or *Mdmx*-Tg BM cells (Ly45.2) and 1.0 × 10⁶ WT competitors (Ly45.1/2) were competitively transplanted into lethally irradiated recipients (Ly45.1). Graph shows ratio of donor cells (Ly45.2) at indicated time points (months) after transplantation for each lineage (n = 10 for WT, 9 for *Mdmx*-Tg). (A–D) Statistical differences were calculated by t test. Data shown as mean ± SEM. *0.01 ≤ p < 0.05, **0.001 ≤ p < 0.01, ***p < 0.001, N.S., not significant. See also Figure S1.

displayed neutrophilia (Figure 2D) and expanded total BM cell counts in comparison with URE^{-/-} mice (Figure 2E), with only a minor increase in blast-like cells (Figure 2F), indicating that these mice were still in a preleukemic stage. Further, the ratio of BM cKit⁺ cells within non-lymphoid cells and the ratio of line-

age⁻ cKit⁺ cells, which includes the pre-LSC/LSC fraction (Steidl et al., 2006), were significantly increased in URE^{-/-}; *Mdmx*-Tg compared with URE^{-/-} mice (Figures 2G, S2B, and S2C). Spleens were also larger in URE^{-/-}; *Mdmx*-Tg compared with URE^{-/-} mice, and they were predominantly composed of

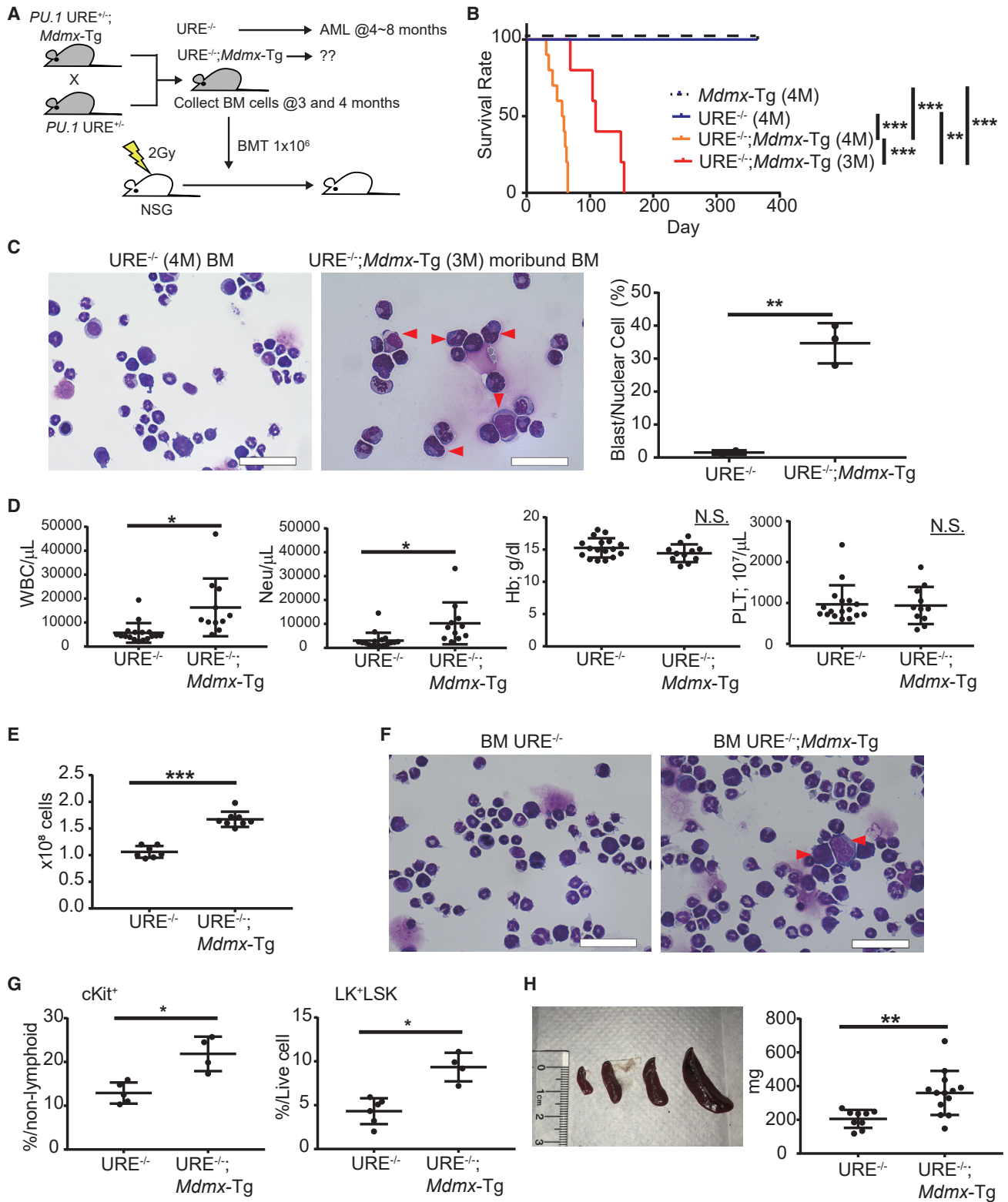


Figure 2. MDMX overexpression transforms *PU.1* knockdown-induced pre-LSC

(A) Schema of the bone marrow transplantation (BMT) assay. BM cells from 3-month-old (3M) *URE*^{-/-}; *Mdmx*-Tg mice (preleukemic), 4-month-old (4M) *URE*^{-/-} mice (preleukemic), or 4M *URE*^{-/-}; *Mdmx*-Tg mice (leukemic) were transplanted into sublethally irradiated NSG mice.

(legend continued on next page)

myeloid cells both in $URE^{-/-};Mdmx-Tg$ and $URE^{-/-}$ mice (Figures 2H and S2D). Overall, MDMX overexpression led to a significantly more aggressive disease with reduced survival of $URE^{-/-};Mdmx-Tg$ primary mice (median 115 days) compared with $URE^{-/-}$ alone (median 178 days) (Figure S2E). Also, moribund $URE^{-/-};Mdmx-Tg$ mice displayed a greatly increased blast percentage in the BM ($URE^{-/-};Mdmx-Tg$; $71.3\% \pm 4.2\%$, compared with $URE^{-/-}$: $21.3\% \pm 4.2\%$, $p < 0.001$) (Figure S2F). In summary, these findings support a concept of MDMX overexpression mediating the transition of pre-LSC to LSC in a model of *PU.1* knockdown-induced preleukemia.

MDMX overexpression induces AML in the *Tet2*^{-/-} myeloproliferative neoplasms/myelodysplastic syndrome model and the *Tet2*^{+/-} clonal hematopoiesis model

Our observations in the context of reduced levels of *PU.1*, a preleukemic driver frequently encountered in patients with myelodysplastic syndrome (MDS) and AML, prompted us to examine other preleukemic and chronic-leukemic murine models for the effects of MDMX overexpression. We utilized *Tet2*-deficient models, as *TET2* mutations represent a frequent early-stage event in patients with myeloproliferative neoplasms (MPNs), MDS, and AML, as well as in individuals with clonal hematopoiesis (CH) (Genovese et al., 2014; Jaiswal et al., 2014). *Tet2*^{-/-} mice have been reported to develop MPN/MDS-like disease with more than 1-year latency, while *Tet2*^{+/-} mice can serve as a CH model with many mice being asymptomatic and a few developing a mild form of MPN (Ko et al., 2011; Moran-Crusio et al., 2011). We crossbred *Tet2*-deficient mice (Ko et al., 2011) with *Mdmx-Tg* mice (Figure 3A). We first compared *Tet2*^{-/-} with *Tet2*^{-/-};*Mdmx-Tg* mice. *Tet2*^{-/-};*Mdmx-Tg* animals died significantly earlier than *Tet2*^{-/-} mice (Figure 3B), and, strikingly, developed an aggressive overt AML presenting with massive splenomegaly with myeloid infiltration, BM infiltration with high blast counts, and expansion of cKit-high myeloid cell and CD48⁺ CD150⁻ LSK cells (Figures 3C–3E). *Tet2*^{-/-} mice only developed an MPN/MDS-like phenotype consistent with prior reports (Figures 3B–3E). In addition, we found that three out of seven mice in our *Tet2*^{+/-};*Mdmx-Tg* cohort developed overt AML at 9, 14, and 17 months of age, while *Tet2*^{+/-} mice did not (Figures 3F–3H). Taken together, MDMX overexpression induces transformation to AML in both a *Tet2*-deficient as well as a *Tet2*-haploinsufficient background.

MDMX overexpression induces AML in the context of asymptomatic heterozygous *Flt3* mutations

We investigated whether MDMX induces leukemic transformation in other non-leukemic genetic models. Heterozygous

FLT3-activating mutations are among the most frequent mutations in AML patients; however, *Flt3*^{WT/ITD} mice do not develop an overt leukemic phenotype and have a life span comparable with WT mice (Lee et al., 2007). We bred *Flt3*^{ITD/ITD} with *Mdmx-Tg* mice to generate *Flt3*^{WT/ITD};*Mdmx-Tg* mice, which we compared with *Flt3*^{WT/ITD} littermate controls (Figure 4A). *Flt3*^{WT/ITD};*Mdmx-Tg* mice died between 6 and 20 months of age (median, 536.5 days), while most of the *Flt3*^{WT/ITD} animals lived more than 24 months (median not reached) (Figure 4B). Moribund *Flt3*^{WT/ITD};*Mdmx-Tg* mice ($n = 5$) exhibited significant increase of white blood cell counts with invasion of blasts and a moderate but significant reduction of platelets relative to age-matched *Flt3*^{WT/ITD} littermates (Figure 4C). The BM of these mice was heavily infiltrated with myeloblasts, while no blast-like cells were observed in *Flt3*^{WT/ITD} BM (Figure 4D). Flow cytometric analysis of BM cells revealed a significant increase in myeloid precursors (cKit⁺ Gr-1⁺) as well as more immature lineage-negative cKit-positive cells, and an increase in CD48⁺ CD150⁻ LSKs in *Flt3*^{WT/ITD};*Mdmx-Tg* (Figure 4E). Spectral karyotyping (SKY) of lineage-negative cKit-positive AML cells revealed the presence of complex chromosomal abnormalities, including deletions, duplications, and translocations, providing evidence for clonality of malignant cells (Figures S3A and S3B). Moribund mice displayed severe splenomegaly (Figure S3C) with the myeloid cell fraction in the spleen markedly increased compared with control littermates (Figure S3D). A group of *Flt3*^{WT/ITD};*Mdmx-Tg* mice, age matched to moribund mice but not overtly sick yet (labeled as non-diseased), were also analyzed and displayed qualitatively similar, but less severe, AML-like changes in the blood, spleen, and BM compared with those of moribund mice (Figures 4C–4E). Taken together, these data revealed that MDMX overexpression combined with the non-penetrant *Flt3*^{WT/ITD} allele triggers leukemic transformation and induces overt AML.

Because of MDMX's function as a p53 inhibitor, we analyzed the coexistence of *FLT3* mutations with *TP53* mutations in human AML cases. Using TCGA datasets, we found that mutations of *FLT3* and *TP53* are mutually exclusive (Figure S3E), consistent with prior reports (Hou et al., 2015; Kadia et al., 2016). On the other hand, MDMX overexpression is observed in the vast majority of AML cases regardless of co-mutations and includes *FLT3*-mutant patients (Carvajal et al., 2018; Han et al., 2016). This prompted us to consider the intriguing possibility of a potential p53-independent function of MDMX overexpression in driving leukemogenesis, which we will describe further below.

(B) Survival after BMT of 1×10^6 BM cells from indicated mice into NSG recipients. $n = 5$ for $URE^{-/-}$ (4M), *Mdmx-Tg*, and $URE^{-/-};Mdmx-Tg$ (3M); $n = 10$ for $URE^{-/-};Mdmx-Tg$ (4M). Statistical significance was calculated by log rank test. **0.001 $\leq p < 0.01$, *** $p < 0.001$.

(C) Left: BM smears of BMT recipients. Right: BM blast counts of the recipients of $URE^{-/-}$ (4M) cells and moribund recipients of $URE^{-/-};Mdmx-Tg$ (3M) cells.

(D) Peripheral blood cell counts from 3M primary mice ($n = 17$ for $URE^{-/-}$, 11 for $URE^{-/-};Mdmx-Tg$). WBC, white blood cell; Neu, neutrophil; Hb, hemoglobin; PLT, platelet.

(E) Total BM cell number from 3M primary mice. Cell numbers were counted from crushed tibia, femur, ileum, sternum, and vertebrae ($n = 7$ for $URE^{-/-}$, 8 for $URE^{-/-};Mdmx-Tg$).

(F) Representative picture of BM cytopsin of 3M primary mice.

(G) Left: ratio of cKit-positive cells in non-lymphoid BM cells of 3M primary mice ($n = 5$ for $URE^{-/-}$, 4 for $URE^{-/-};Mdmx-Tg$). Right: ratio of live lineage⁻ cKit⁺ cells (LK [lineage⁻ cKit⁺] and LSK) in the BM.

(H) Left: representative image of spleens from 3M primary mice. The order of the genotypes is WT, $URE^{-/-}$, $URE^{-/-};Mdmx-Tg$, $URE^{-/-};Mdmx-Tg$ (moribund) from left to right. Right: spleen weights of 3M primary mice ($n = 9$ for $URE^{-/-}$, 13 for $URE^{-/-};Mdmx-Tg$). # (C)–(F) Arrowheads indicate blast cells. Scale bars: 40 μ m. # (C–E, G, H) statistical significance was calculated by t test. Data shown as mean \pm SEM. *0.01 $\leq p < 0.05$, **0.001 $\leq p < 0.01$, *** $p < 0.001$. See also Figure S2.

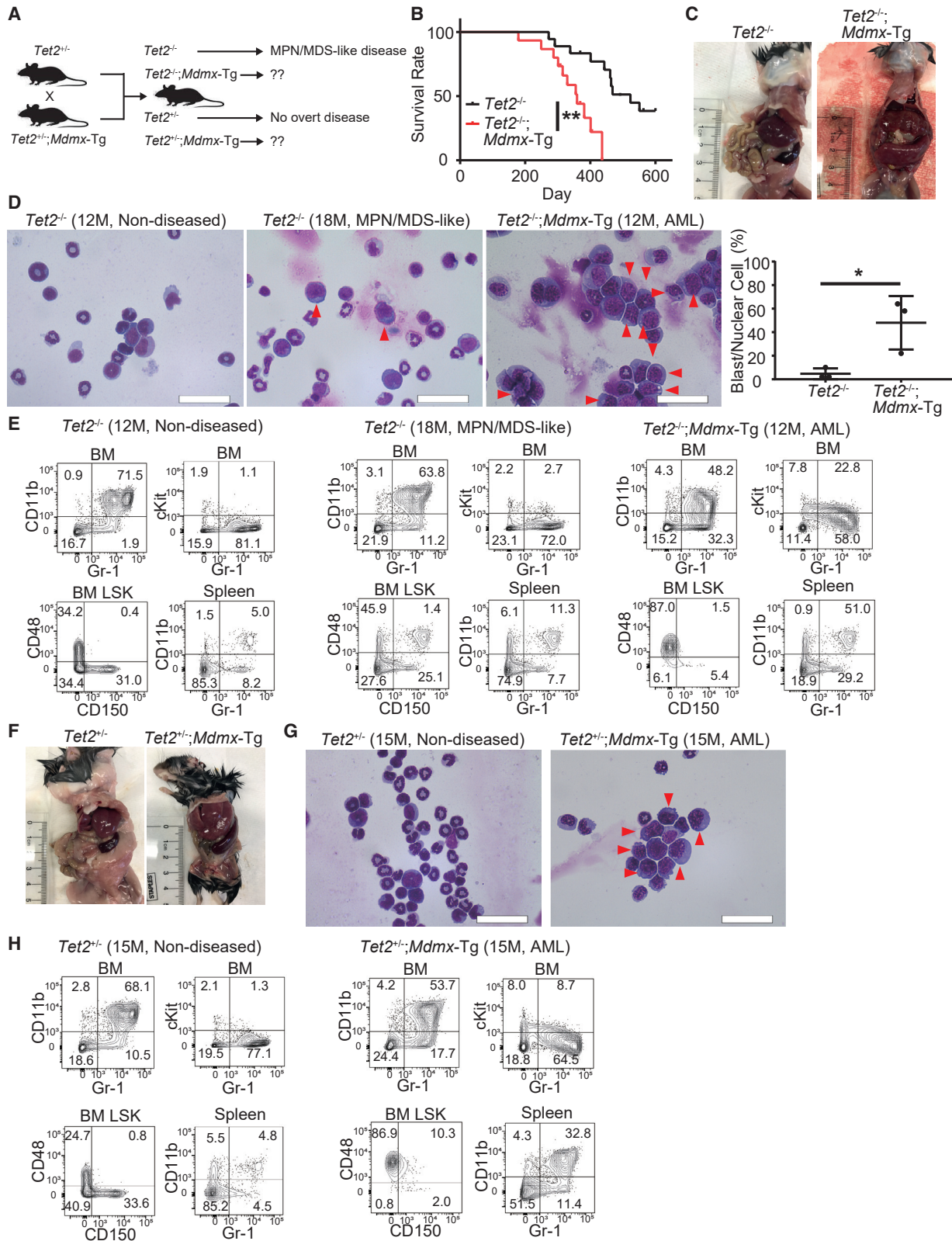


Figure 3. MDMX overexpression induces AML in the *Tet2*^{-/-} MPN/MDS model and *Tet2*^{+/-} CH model

(A) Schema of the breeding strategy, resultant genotypes and phenotypes.

(B) Survival of *Tet2*^{-/-} and *Tet2*^{+/-}; *Mdmx*-Tg mice (n = 15 for *Tet2*^{-/-}, 18 for *Tet2*^{+/-}; *Mdmx*-Tg). **0.001 ≤ p < 0.01 by log rank test.

(legend continued on next page)

MDMX overexpression triggers AML in the context of *Nras*-G12D-driven chronic myelomonocytic disease

To further establish the contribution of MDMX overexpression to AML onset, we expanded our studies to an additional model of a slowly progressing, chronic myeloid disease, driven by the *Nras*-G12D mutation. Adoptive transfer of *Nras*-G12D-transduced BM cells leads to a chronic myelomonocytic leukemia (CMML)-like disease at around 6 months post transplantation (Parikh et al., 2007). We retrovirally introduced the *Nras*-G12D mutant into cKit⁺ WT or *Mdmx*-Tg BM cells (transduction efficiency, 19% ± 1%), followed by transplantation into lethally irradiated C57BL/6 recipients (Figure S4A). Recipients of *Nras*-G12D *Mdmx*-Tg cells (*Nras*^{G12D};*Mdmx*-Tg) rapidly succumbed to disease within around 2 months after transplantation (median, 67 days), while *NRAS*-G12D recipients (*Nras*^{G12D}) developed disease at 4 to 8 months after transplantation (median, 153 days) (Figure S4B). Several of the *Nras*^{G12D};*Mdmx*-Tg mice we analyzed showed BM invasion of GFP⁺ CD11b⁺ Gr-1⁺ cKit^{dim} AML-like cells (Figure S4C). In *Nras*^{G12D} mice, there were no detectable GFP-positive tumor cells in the BM at 2 months after transplantation; however, by 5 months there was infiltration with GFP⁺ CD11b⁺ Gr-1⁻ cKit^{low} monocytic cells, which is compatible with CMML-like disease and consistent with prior reports (Figure S4C) (Parikh et al., 2007; Zhang et al., 2017). Moreover, severe hepatosplenomegaly was observed in all *Nras*^{G12D};*Mdmx*-Tg mice at 2 months, while the spleen weight of *Nras*^{G12D} mice was normal at the analyzed time point (Figure S5A). The GFP⁺ cells from G12D spleens and BM at 5 months were CD11b⁺ Gr-1⁻ monocytic cells, reflecting a CMML-like phenotype (Figure S5B and S5C). However, the GFP⁺ spleen cells of *Nras*^{G12D};*Mdmx*-Tg mice additionally displayed acute leukemia phenotypes: either Gr-1⁻ CD11b⁻ CD8⁺ and Gr-1⁻ CD11b⁺ CD8⁺ co-existing bulk tumor cells (i.e., CMML/AML + T cell acute lymphoblastic leukemia [T-ALL]) or Gr-1⁻ CD11b⁺ and Gr-1⁺ CD11b⁺ cKit⁺ co-existing bulk tumor cells (i.e., CMML + AML type) (Figure S5C). GFP⁺ thymus cells from *Nras*^{G12D};*Mdmx*-Tg mice with the combined myeloid plus T-ALL phenotype showed CD8⁺ skewed lymphopoiesis, and they contained an altered CD8/CD4 double-negative (DN) fraction (Figure S5D). These observations support a co-diagnosis of murine T-ALL/thymotic lymphoma in some animals (Tremblay et al., 2010), in addition to the AML phenotype present in all *Nras*^{G12D};*Mdmx*-Tg recipients (Figure S5E).

In summary, our studies demonstrate that MDMX overexpression leads to a transition from non-penetrant, or slowly progressing, chronic myeloid disease to overt acute myeloid leukemia in five different genetic models, including PU.1 *URE*^{-/-};*Mdmx*-Tg, *Tet2*^{-/-};*Mdmx*-Tg, *Tet2*^{+/-};*Mdmx*-Tg, *Flt3*^{WT/ITD};*Mdmx*-Tg, and *Nras*^{G12D};*Mdmx*-Tg.

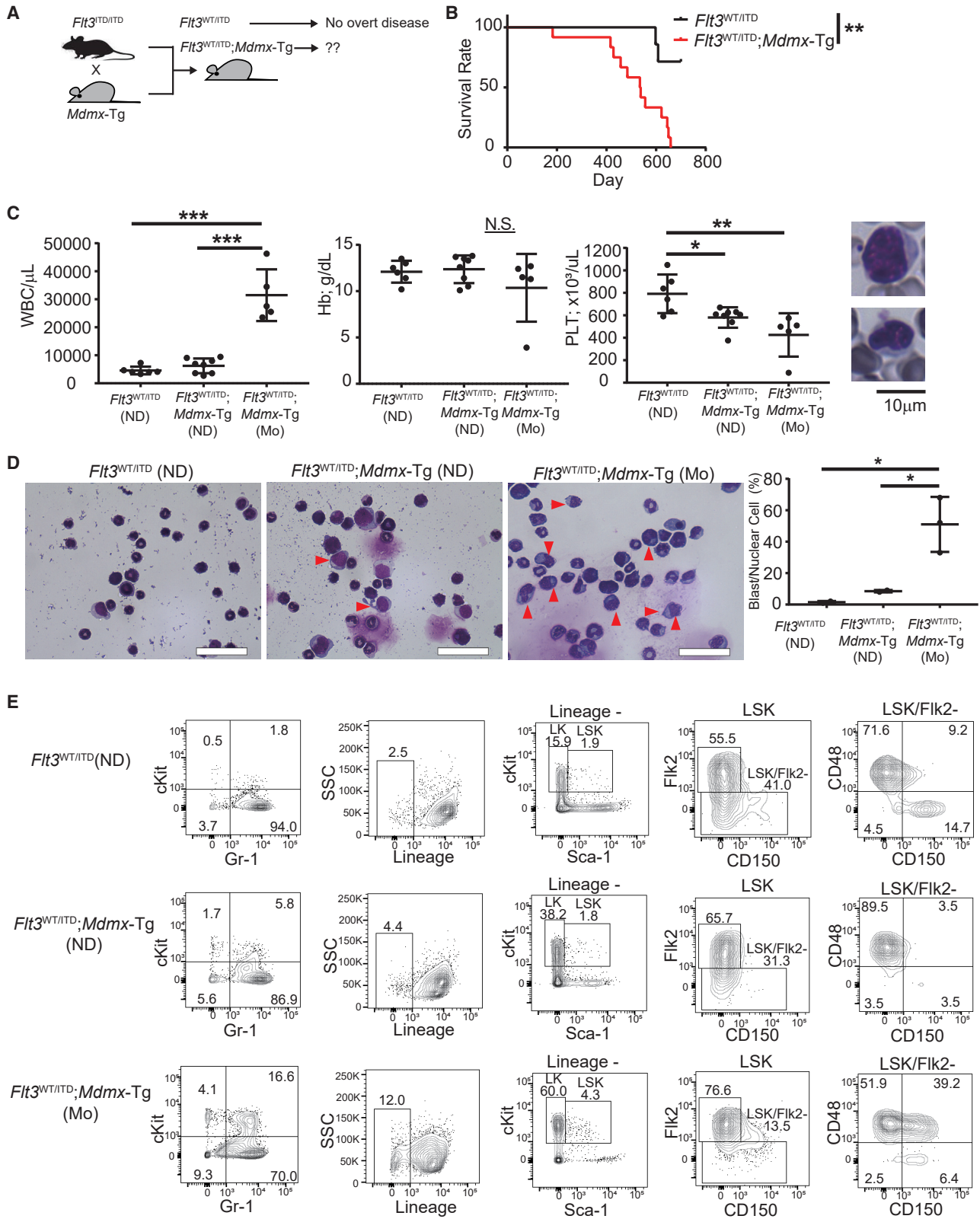
MDMX overexpression leads to upregulation of Wnt/ β -Catenin signaling in pre-LSC, an effect that is mediated by physical interaction of MDMX with CK1 α

Our finding of cooperativity of MDMX overexpression in the context of *Flt3* mutation, combined with the clinical observation of mutual exclusivity of *FLT3* and *TP53* mutations, raised the interesting possibility of p53-independent mechanisms playing a role in the AML-triggering effects of MDMX overexpression. To study the possible underlying molecular mechanisms, we performed both RNA sequencing (RNA-seq) as well as immunoprecipitation (IP) followed by mass spectrometry (liquid chromatography-tandem mass spectrometry [LC-MS/MS]) experiments.

HSCs (Flk2⁻ LSK) from WT and *Mdmx*-Tg mice, and pre-LSCs (Flk2⁻ LSK) from *URE*^{-/-} and *URE*^{-/-};*Mdmx*-Tg mice were transcriptionally interrogated via RNA-seq (Tables S1 and S2). As expected, expression of p53 targets was repressed in *Mdmx*-Tg HSCs compared with WT HSCs; however, only to a relatively modest extent (NES [normalized enrichment score], -1.15; p = 0.25) (Figure 5A). Interestingly, using ingenuity pathway analysis (IPA), we found that Wnt/ β -Catenin was the most significantly upregulated canonical pathway (Z score, 1.6; p = 0.006) (Figure 5B). Gene set enrichment analysis (GSEA) also revealed a *Ctnnb1* (β -Catenin) oncogenic signature to be upregulated in *Mdmx*-Tg HSCs (NES, 1.52; p = 0.04) (Figure 5C). RNA-seq comparison of *URE*^{-/-} versus *URE*^{-/-};*Mdmx*-Tg pre-LSC also exhibited upregulated *Ctnnb1* oncogenic (NES, 1.36; p = 0.059) and Wnt/ β -Catenin signaling signatures (NES, 1.41; p = 0.072) (Figure 5E). In addition to upregulation of the Wnt/ β -Catenin pathway, the suppression of p53 targets and apoptosis pathways was evident in *URE*^{-/-};*Mdmx*-Tg pre-LSC (NES, -1.68; p = 0.004. NES, -1.40; p = 0.016, respectively) (Figure 5D). We confirmed increased levels of β -Catenin protein by immunofluorescence (IF) staining in *Mdmx*-Tg, *URE*^{-/-};*Mdmx*-Tg, and *Tet2*^{+/-};*Mdmx*-Tg HSC/pre-LSC (Figures 5F and S6A).

Next, we set out to identify proteins that interact with MDMX in myeloid cells. We transduced the p53-WT/MDMX-low murine AML cell line 32D with an HA-tagged murine MDMX-expressing lentiviral vector (Figure 5G). We extracted total cellular protein and performed MDMX-interactome screening using IP against the HA-tag followed by mass spectrometry (LC-MS/MS). Among all interacting proteins, casein kinase CK1 α (*Csnk1a1*) was the top, non-structural/non-housekeeping MDMX-interacting protein in 32D AML cells (Table S3, Figure S6B). This appeared to be of particular interest to us as previous studies had reported that CK1 α can bind and regulate both MDMX and β -Catenin in other cell types (Chen et al., 2005; Liu et al., 2002; Wu et al., 2012). We therefore focused on the possible interaction of MDMX with CK1 α and its

- (C) Abdominal cavity of moribund *Tet2*^{-/-};*Mdmx*-Tg mouse and a *Tet2*^{-/-} littermate reveals drastic hepatosplenomegaly in the *Tet2*^{-/-};*Mdmx*-Tg mouse.
 (D) Left: BM cytopspins of a non-diseased *Tet2*^{-/-} mouse at 12 months of age (12M), a moribund (MPN/MDS-like) *Tet2*^{-/-} mouse at 18 months of age (18M), and a moribund (AML) *Tet2*^{-/-};*Mdmx*-Tg mouse at 12M. Right: percentage of blasts in the BM cells of moribund *Tet2*^{-/-};*Mdmx*-Tg and *Tet2*^{-/-} mice. Bars indicate mean ± SEM. *0.01 ≤ p < 0.05 by t test.
 (E) Flow cytometric analysis of BM/spleen cells of a non-diseased *Tet2*^{-/-} mouse (12M), a moribund (MPN/MDS-like) *Tet2*^{-/-} mouse (18M), and a moribund (AML) *Tet2*^{-/-};*Mdmx*-Tg mouse (12M).
 (F) Abdominal cavity of a moribund *Tet2*^{+/-};*Mdmx*-Tg mouse and its littermate (*Tet2*^{+/-}).
 (G) BM cytopspins of a moribund (AML) *Tet2*^{+/-};*Mdmx*-Tg mouse (15 months old [15M]) and a *Tet2*^{+/-} littermate.
 (H) Flow cytometric analysis of BM and spleen cells of a moribund *Tet2*^{+/-};*Mdmx*-Tg mouse and a *Tet2*^{+/-} littermate. # (D and G) Arrows indicate morphological blasts. Scale bars: 40μm.



(legend on next page)

downstream effects on Wnt/ β -Catenin signaling in leukemia/preleukemia cells. Using coIP assays followed by western blotting (WB), we validated the LC-MS/MS results and found that MDMX indeed interacts with CK1 α in AML cells (Figure 5H). We further hypothesized that this interaction may prevent CK1 α binding to β -Catenin upon MDMX overexpression. In agreement with this hypothesis, we found that total protein expression as well as nuclear import of β -Catenin was increased in 32D cells upon MDMX overexpression (Figure 5H); at the same time, RNA expression levels of *Ctnnb1* remained unchanged (Figure 5I), indicating that β -Catenin is regulated at the protein level. Also, overexpression of CK1 α in MDMX-overexpressing 32D cells reduced expression and nuclear transportation of β -Catenin (Figure S6C), indicating that CK1 α abundance plays a causative role in the MDMX-mediated elevation of β -Catenin levels. Collectively, our results indicate that MDMX binds to and reduces cellular abundance of CK1 α in AML cells and, as a consequence, leads to increased nuclear levels of β -Catenin.

Wnt/ β -Catenin inhibition or elevation of CK1 α levels rescue MDMX-overexpression-induced functional properties of pre-LSC

We next investigated whether the observed elevation of β -Catenin signaling and sequestration of CK1 α are functionally relevant in MDMX-overexpressing pre-LSCs. For this purpose, we first utilized two pharmacological inhibitors of Wnt/ β -Catenin, WNT974 and PNU74654. WNT974 is a porcupine inhibitor that prevents the secretion of Wnt, hence it broadly inhibits Wnt/ β -Catenin signaling (Liu et al., 2013), while PNU74654 inhibits the interaction of nuclear β -Catenin with transcription factors and suppresses canonical Wnt/ β -Catenin signaling (Trosset et al., 2006). Colony-forming assays showed that WT HSCs tolerated Wnt/ β -Catenin inhibition well (half maximal inhibitory concentrations [IC50s]: 13.7 μ M for WNT974, >20 μ M for PNU74654) except at very high concentrations of WNT974 (Figure 6A), in line with a previous study demonstrating that canonical Wnt/ β -Catenin signaling is largely dispensable for adult hematopoiesis (Cobas et al., 2004). On the other hand, *Mdmx*-Tg HSCs were significantly more sensitive (IC50s: 0.1 μ M for WNT974, 0.5 μ M for PNU74654) to both the Wnt/ β -Catenin inhibitors, including at nanomolar concentrations (Figure 6A).

Next, we investigated whether retroviral overexpression of CK1 α in cKit⁺ HSPCs also affected colony-forming ability of MDMX-overexpressing cells in a similar manner. We transduced WT or *Mdmx*-Tg HSPCs with an MSCV-CK1 α (*Csnk1a1*)-IRES-GFP (Jaras et al., 2014) or Empty vector and performed serial replating assays. Strikingly, CK1 α overexpression indeed resulted in complete suppression of colony formation of *Mdmx*-Tg

HSPCs after the third replating, while Empty vector-transduced *Mdmx*-Tg HSPCs maintained high colony-forming capacity (Figure 6B). Moreover, we did not observe any significant change in serial replating capacity of WT HSPCs upon CK1 α overexpression.

Similarly, *URE*^{-/-}; *Mdmx*-Tg and *Flt3*^{WT/ITD}; *Mdmx*-Tg pre-LSCs were sensitive to Wnt/ β -Catenin inhibition by WNT974 and PNU74654, while *URE*^{-/-} and *Flt3*^{WT/ITD} pre-LSCs were not (Figures 6C and S7A). Likewise, CK1 α overexpression rescued the increased colony-forming ability of *URE*^{-/-}; *Mdmx*-Tg as well as *Flt3*^{WT/ITD}; *Mdmx*-Tg, whereas *URE*^{-/-} and *Flt3*^{WT/ITD} pre-LSCs were not significantly affected (Figures 6D and S7B). Also, knock-down of β -Catenin (*Ctnnb1*) in LSCs (lineage⁻ cKit⁺ cells in *URE*^{-/-}; *Mdmx*-Tg leukemic mice) remarkably reduced colony formation, while reduction of colony by *Ctnnb1* knockdown was limited in LSCs of *URE*^{-/-} mice (Figure S7C).

Altogether, these findings using different model systems demonstrate that increased Wnt/ β -Catenin signaling is, at least in part, mediating the increase in colony-forming capacity of MDMX-overexpressing pre-LSCs/LSCs. Furthermore, our data demonstrate that CK1 α overexpression can abrogate the increased serial replating capacity of MDMX overexpression-induced pre-LSC.

In a next step, we explored the potential utility of our findings for possible combinatorial therapy. Specifically, we investigated whether combination of a Wnt/ β -Catenin inhibitor (PNU74654) and ALRN-6924, which re-activates p53 by inhibiting interaction of MDMX with TP53 protein (Carvajal et al., 2018), would be beneficial. We found that *URE*^{-/-}; *Mdmx*-Tg preleukemic lineage⁻ cKit⁺ cells were only modestly sensitive to single-drug treatment by either PNU74654 or ALRN-6924. However, the combination of PNU74654 and ALRN-6924 showed strong synergy in eradicating *URE*^{-/-}; *Mdmx*-Tg pre-LSCs (Figure 6E, left), and the combination index (CI) indicated substantially stronger synergism in *URE*^{-/-}; *Mdmx*-Tg cells (CI = 0.12) compared with WT (CI = 0.59) or *URE*^{-/-} (CI = 0.56) controls (Figure 6E, right). We next tested the combination treatment *in vivo*, and injected ALRN-6924 and BC2059 (a Wnt/ β -Catenin inhibitor suitable for *in vivo* studies) into recipient mice of 3-month-old *URE*^{-/-}; *Mdmx*-Tg cells (which leads to AML in recipients). While single-drug treatment with either ALRN-6924 or BC2059 slightly prolonged survival, combination treatment with both drugs was significantly more effective (Figure S7D). Moreover, we found that treatment with Wnt/ β -Catenin inhibitor sensitized a previously reported ALRN-6924-resistant human AML cell line, OCI-AML3 (p53-WT), to ALRN-6924 treatment (CI: 0.17) (Figure S7E). Collectively, these data suggest that the MDMX/CK1 α / β -Catenin axis in pre-LSC, which our mechanistic studies revealed, is therapeutically targetable.

Figure 4. MDMX overexpression induces AML in the context of asymptomatic heterozygous *Flt3* mutations

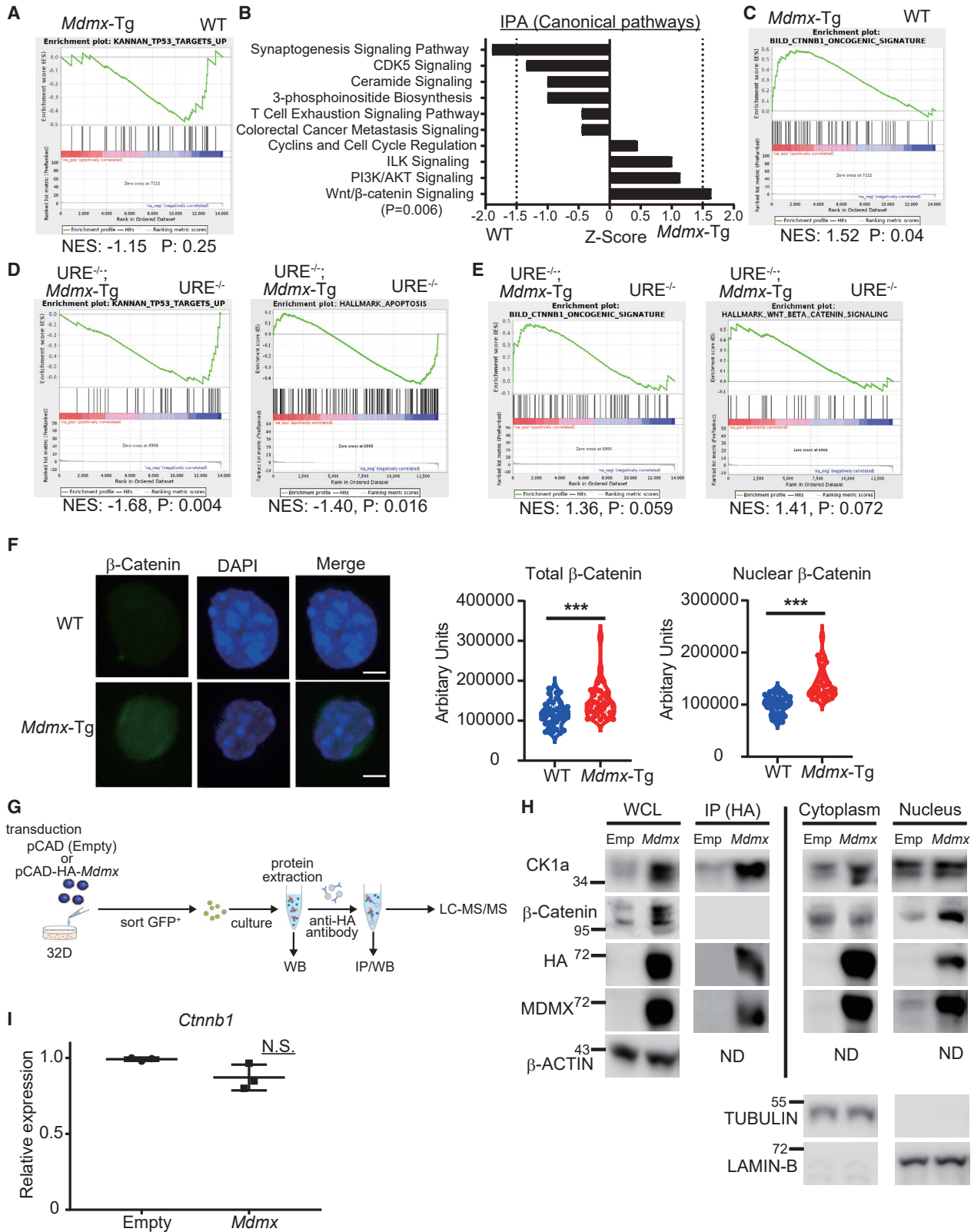
(A) Schema of the breeding strategy of *Flt3*^{WT/ITD}; *Mdmx*-Tg mice.

(B) Survival of *FLT3*^{WT/ITD} and *Flt3*^{WT/ITD}; *Mdmx*-Tg mice (n = 7 for *FLT3*^{WT/ITD}, 12 for *Flt3*^{WT/ITD}; *Mdmx*-Tg). **0.001 \leq p < 0.01 by log rank test.

(C) Left: peripheral blood counts of moribund (Mo) mice and 16-month-old non-diseased (ND) mice. n = 6 for *FLT3*^{WT/ITD} (ND), 8 for *Flt3*^{WT/ITD}; *Mdmx*-Tg (ND), 5 for *Flt3*^{WT/ITD}; *Mdmx*-Tg (Mo). Statistics were calculated by Tukey HSD (honestly significant difference) test. Data shown as mean \pm SEM. *0.01 \leq p < 0.05, **0.001 \leq p < 0.01, ***p < 0.001. Right: representative blasts in peripheral blood.

(D) Left: BM cytopsin from Mo or age-matched ND mice. Scale bars: 40 μ m. Arrowheads indicate blast cells. Right: percentage of blasts among nuclear cells (n = 2, 2, 3 respectively). Statistics were calculated by Tukey HSD test. Data shown as mean \pm SEM. *0.01 \leq p < 0.05.

(E) Representative flow cytometric analysis of BM of Mo mice and 16-month-old ND mice. See also Figures S3–S5.



(legend on next page)

MDMX-driven HSC expansion and Wnt/ β -Catenin upregulation is p53 independent

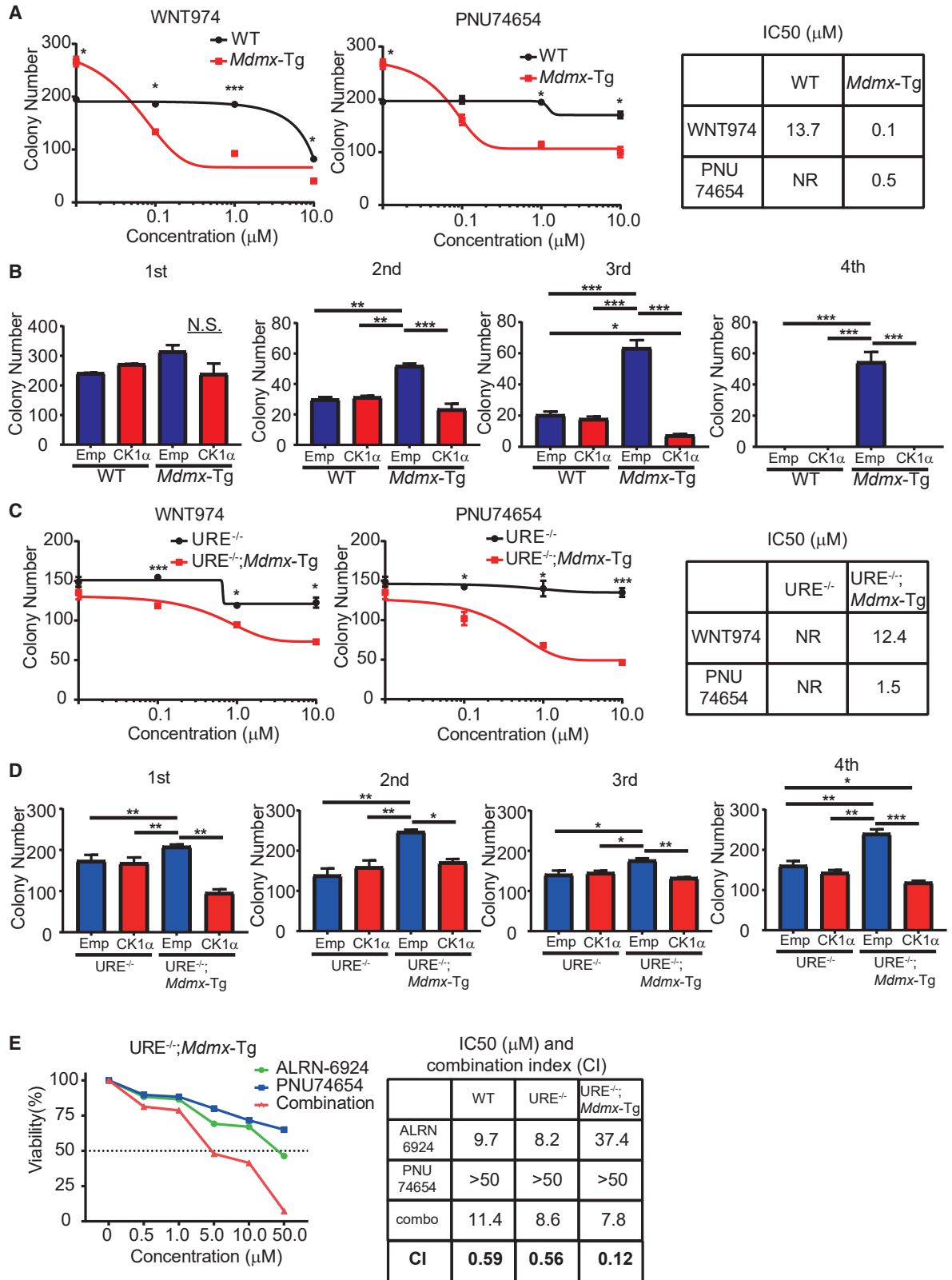
Next, we asked whether β -Catenin upregulation and resultant functional effects in an MDMX overexpression background are p53 dependent or not. We therefore generated *Mdmx*-Tg mice in a p53 null background (*Trp53*^{-/-};*Mdmx*-Tg). HSCs of *Trp53*^{-/-};*Mdmx*-Tg mice overexpressed *Mdmx* 20.3-fold \pm 2.4-fold compared with *Trp53*^{-/-} (Figure 7A), and we found that *Trp53*^{-/-};*Mdmx*-Tg BM cells had significantly higher serial replating capacity compared with *Trp53*^{-/-} (Figure 7B). We then transplanted *Trp53*^{-/-} or *Trp53*^{-/-};*Mdmx*-Tg (Ly45.2) BM cells together with WT competitor cells (Ly45.1/2) into lethally irradiated C57BL/6 recipients (Ly45.1). *Trp53*^{-/-};*Mdmx*-Tg cells reconstituted the myeloid lineage to a significantly greater extent than *Trp53*^{-/-} cells (Figure 7C); however, unlike the *Mdmx*-Tg versus WT competitive transplantation assay (Figure 1D), reconstitution of the lymphoid lineage did not differ between *Trp53*^{-/-} and *Trp53*^{-/-};*Mdmx*-Tg. In addition, mice who received *Trp53*^{-/-};*Mdmx*-Tg cells displayed a higher proportion of LSK cells than *Trp53*^{-/-} recipients (Figure 7C). We concluded that MDMX overexpression enhances competitiveness of HSCs and specifically myeloid reconstitution independent of its functions involving p53. We also found protein levels of β -Catenin (both total as well as nuclear) and RNA expression of its major targets, *Ccnd1* and *c-Myc*, to be significantly increased in *Trp53*^{-/-};*Mdmx*-Tg HSCs (Figures 7D and 7E). In line with this, we found the colony-forming ability of *Trp53*^{-/-};*Mdmx*-Tg HSCs to be impaired by treatment with the canonical Wnt/ β -Catenin inhibitor PNU74654, while *Trp53*^{-/-} HSCs were unaffected (Figure 7F). Lastly, we overexpressed FLAG-tagged MDMX in the p53-null human AML cell line HL-60. While RNA expression of *CTNNB1* was not different between Empty vector and MDMX transduced cells (Figure 7G), we found increased expression of β -Catenin protein in whole-cell lysates as well as cytoplasmic and nuclear extracts from MDMX-overexpressing HL-60 cells (Figure 7H). Furthermore, we detected interaction of MDMX and CK1 α in the p53-null context (Figure 7H). In summary, these data reveal that MDMX overexpression leads to expansion of the HSC compartment, and specifically enhances their reconstitution of the myeloid lineage, in a p53-independent manner. At the mechanistic level, the physical interaction of MDMX with CK1 α is also not dependent on p53.

Clinical-correlative data indicate relevance of the MDMX-Wnt/ β -Catenin axis in patients with MDS

We analyzed large published patient cohorts to examine the potential clinical relevance of the MDMX/ β -Catenin axis. As our data suggests that Wnt/ β -Catenin upregulation by MDMX overexpression is important for leukemic transformation from a preleukemic stage, we focused on a cohort of patients with non-treated MDS for which both molecular as well as clinical time-to-event data were available (GSE19429). We dichotomized patients into MDMX-high and MDMX-low expressers, and found enrichment of a Wnt/ β -Catenin signature in patients with high MDMX expression (Figure 8A). The mutation status of CH-related genes was comparable in both the MDMX-high and MDMX-low groups, except for *SRSF2* (Figure 8B). Interestingly, MDMX-high patients included more refractory anemia with excess blasts (RAEB) cases, which is a more severe subtype of MDS (Figure 8C). In a next step, we evaluated cumulative incidence of transformation to AML treating non-leukemic death as competing risk. Strikingly, MDS patients with high MDMX expression displayed a higher transformation rate to AML in the entire cohort compared with patients with low MDMX expression (Figure 8D), but also when we analyzed patients with RAEB (Figure 8E) and patients with non-RAEB subtype (Figure 8F) separately, while non-leukemic death was not significantly different in all subgroups. Moreover, patients who were simultaneously MDMX high as well as WNT score (Bhagat et al., 2017) high showed very rapid progression to AML, and this transformation rate was highly significantly different compared with all other patients (Figure 8G). Patients with RAEB showed no significant difference in blast percentage between the MDMX-low versus -high groups (10.25% \pm 4.00%, and 12.16% \pm 4.60%, respectively). We next investigated primary BM samples of MDS. About half of MDS RAEB cases had elevated MDMX, about 5- to 6-fold increased levels compared with normal (Figure S8A), and HSPCs (lineage⁻/CD34⁺) from MDMX-high patients were significantly more sensitive to treatment with β -Catenin inhibitor (Figure S8B), consistent with our previous findings in murine models. Taken together, these data suggest that the MDMX-Wnt/ β -Catenin axis is functionally important in patients with MDS and relevant for the clinical course of preleukemic disease.

Figure 5. MDMX overexpression leads to upregulation of Wnt/ β -Catenin signaling in pre-LSC, an effect that is mediated by physical interaction of MDMX with CK1 α

- (A) RNA-seq data of WT and *Mdmx*-Tg HSCs analyzed by GSEA for p53 targets. (n = 3).
 (B) Canonical pathways representing the top 10 Z scores by IPA of the RNA-seq data.
 (C) RNA-seq data of WT and *Mdmx*-Tg HSCs were analyzed by GSEA for oncogenic β -Catenin signature.
 (D) RNA-seq of pre-LSCs from *URE*^{-/-} and *URE*^{-/-};*Mdmx*-Tg was performed (n = 3), including GSEA analysis of p53 targets and apoptosis.
 (E) GSEA analysis for β -Catenin oncogenic signature and hallmark Wnt/ β -Catenin signaling for *URE*^{-/-} and *URE*^{-/-};*Mdmx*-Tg.
 (F) Left: protein expression of β -Catenin (green) by IF staining with DAPI (blue) counterstain in HSCs of WT and *Mdmx*-Tg mice. Representative pictures are shown (scale bars: 1.85 μ m). Center: signal of total cell staining of β -Catenin. Right: nuclear signal of β -Catenin with DAPI counterstain. Statistics were calculated by t test. ***p < 0.001.
 (G) Schema of experimental strategy to detect MDMX-interacting proteins.
 (H) Whole-cell lysate (WCL) and cytoplasmic and nuclear proteins were extracted from 32D cells transduced with HA-tagged *Mdmx* or Empty control lentivirus. IP with anti-HA beads was performed for WCL. Samples were blotted for indicated antibodies. Molecular weight (kDa) is indicated in the figure.
 (I) Relative expression of *Cttnb1* RNA in 32D cells transduced with *Mdmx* or Empty control lentivirus (n = 3). Statistical significance was calculated by t test. Data shown as mean \pm SEM. See also Figure S6 and Tables S1, S2, and S3.



(legend on next page)

DISCUSSION

Our studies of MDMX overexpression in murine hematopoiesis revealed an important and pervasive role of MDMX in the induction of AML in the context of several different molecular aberrations frequently occurring in human leukemia. *MDMX* overexpression is detected in almost 90% of AML patients irrespective of mutational subtypes (Carvajal et al., 2018; Han et al., 2016; Quintas-Cardama et al., 2017). The different preleukemic models we combined with *Mdmx* transgenic overexpression act via distinct molecular mechanisms and reflect aberrations that occur frequently in patients. PU.1 inactivation has been previously classified as a so-called class II (i.e., differentiation blocking) aberration that is caused by various genetic, epigenetic, and posttranslational mechanisms and is encountered in 60%–70% of all AML patients (Gilliland and Tallman, 2002; Sive et al., 2016; Tenen, 2003; Will et al., 2015). *TET2* loss-of-function mutations are frequent preleukemic alterations, including in individuals with CH (~10%) (Genovese et al., 2014; Jaiswal et al., 2014). Heterozygous *FLT3* or *NRAS* mutations are two of the most frequent genetic aberrations in AML, and are thought to primarily act as “proliferative hits” and at a later stage in many patients (Bacher et al., 2006; Papaemmanuil et al., 2016) (i.e., class I aberrations) (Bacher et al., 2006; Gilliland and Tallman, 2002; Kiyoi et al., 1999; Nakao et al., 1996; Sive et al., 2016; Staber et al., 2014). Of note, heterozygous *Tet2* and *Flt3* mutations are not sufficient to induce hematopoietic malignancy, and *Nras* mutations only lead to a smoldering MDS/CMML-like phenotype in mice. Furthermore, *MDMX* overexpression occurs in the majority of patients with *TET2*, *FLT3*, or *NRAS*-G12D heterozygous mutations (Cancer Genome Atlas Research Network et al., 2013). Overall, our new MDMX-driven models and findings cover and are applicable to a range of different leukemogenic genetic contexts and mechanisms that are frequently encountered in patients.

Notably, each of the murine models we tested do not develop overt AML as a stand-alone and without MDMX overexpression, while representing classic preleukemic or CH-like conditions (*Tet2* [haplo]insufficiency and PU.1^{low}, respectively) or changes that are associated with myeloproliferative conditions (*Tet2* [homozygous] deficiency, heterozygous *Flt3*-ITD mutations, and *Nras* mutations). In either situation, MDMX was causative in the induction of an acute leukemia phenotype. Since our models do not allow the timely control of induction of the different aberrations, it will be interesting to test in future studies whether the exact timing of MDMX overexpression is critical (early versus late), and may depend on the specific cooperating aberrations.

Our cooperativity models with overexpression of the *Mdmx* transgene showed marked molecular and phenotypic differences from previously studied combinatorial phenotypes with p53 mutants (Dumble et al., 2007). Most importantly, we observed greater competitive advantage of *Trp53*^{-/-};*Mdmx*-Tg compared with *Trp53*^{-/-} cells, indicating that MDMX exerts p53-independent mechanisms of clonal expansion. Furthermore, we found only modest suppression of p53 target genes in MDMX-overexpressing HSCs, which is in contrast to the strong suppression of p53 targets, including cellular quiescence-related genes, that has been previously reported in *Trp53*^{-/-} HSCs (Liu et al., 2009).

Using approach RNA-seq and proteomic studies, we found, unexpectedly, that upregulation of Wnt/β-Catenin signaling in *Mdmx*-Tg mice plays an important role in the expansion of HSCs. We also observed activation of Wnt/β-Catenin signaling in MDMX-overexpressing pre-LSCs, as well as clinical-correlative evidence that *MDMX* expression levels correlate with Wnt/β-Catenin signature in patients with MDS. Wnt/β-Catenin signaling has previously been reported to be implicated in various cancers, including AML (Gruszka et al., 2019; Zhan et al., 2017). On the other hand, canonical Wnt/β-Catenin signaling is dispensable in adult hematopoiesis (Cobas et al., 2004), but its constitutive activation leads to increased cell cycling of HSCs (Scheller et al., 2006), which is consistent with our findings in the MDMX overexpression setting.

Our findings revealed the mechanism of Wnt/β-Catenin signaling upregulation by MDMX overexpression to be the result of physical interaction with and reduced abundance of CK1α, which phosphorylates β-Catenin. CK1α is known to act as a tumor suppressor by phosphorylating β-Catenin on Ser45. This phosphorylation is required for further phosphorylation by GSK3β and subsequent protease-mediated degradation of β-Catenin in the cytoplasm (Liu et al., 2002). Our data indicate that MDMX binds CK1α, thereby preventing its function to phosphorylate β-Catenin and subsequent degradation. CK1α overexpression counteracted the β-Catenin upregulation in MDMX-overexpressing cells and rescued the repopulating phenotypes of *Mdmx*-Tg HSCs/pre-LSCs. Our findings are in line with several reports in other cell types. It has been reported that during the DNA damage response in ES cells, reduced abundance of CK1α activates Wnt/β-Catenin signaling via increased β-Catenin protein levels (Carreras Puigvert et al., 2013); further, CK1α agonists have shown activity against Wnt/β-Catenin-dependent solid tumors via enhanced degradation of β-Catenin (Li et al., 2017). Although CK1α harbors multiple functions (Jiang et al., 2018a), our findings demonstrate that regulation of β-Catenin is a critical role of CK1α in preleukemic and leukemic cells; our

Figure 6. Wnt/β-Catenin inhibition or elevation of CK1α levels rescue MDMX-overexpression-induced functional properties of pre-LSC

- (A) IC50 determination in colony-formation assays of 1,000 WT or *Mdmx*-Tg HSCs with indicated concentration of Wnt/β-Catenin inhibitors (n = 2).
 (B) Colony numbers from 5,000 WT or *Mdmx*-Tg cKit⁺ BM cells transduced with *Csnk1a1* (CK1α) or Empty vector (Emp) (n = 2). Cells were serially replated three times.
 (C) Colony number from 10,000 URE^{-/-} or URE^{-/-};*Mdmx*-Tg pre-LSCs with indicated concentration of Wnt/β-Catenin inhibitors (n = 2).
 (D) Colony number from 5,000 URE^{-/-} or URE^{-/-};*Mdmx*-Tg lineage-cKit⁺ BM cells transformed with *Csnk1a1* (CK1α) or Empty (Epm) vector (n = 2). Cells were serially replated three times.
 (E) IC50 assays of lineage⁻ cKit⁺ BM cells from WT, URE^{-/-}, and URE^{-/-};*Mdmx*-Tg preleukemic mice cultured with the indicated concentrations of PNU74654, ALRN-6924, or both, for 24 h # (A and C) Statistical significance was calculated by t test for each drug concentration. Data shown as mean ± SEM. *0.01 ≤ p < 0.05, **0.001 ≤ p < 0.01, ***p < 0.001. NR, not reached. # (B and D) Statistical significance was calculated by Tukey HSD test. Data shown as mean ± SEM. *0.01 ≤ p < 0.05, **0.001 ≤ p < 0.01, ***p < 0.001. See also Figures S7 and S8.

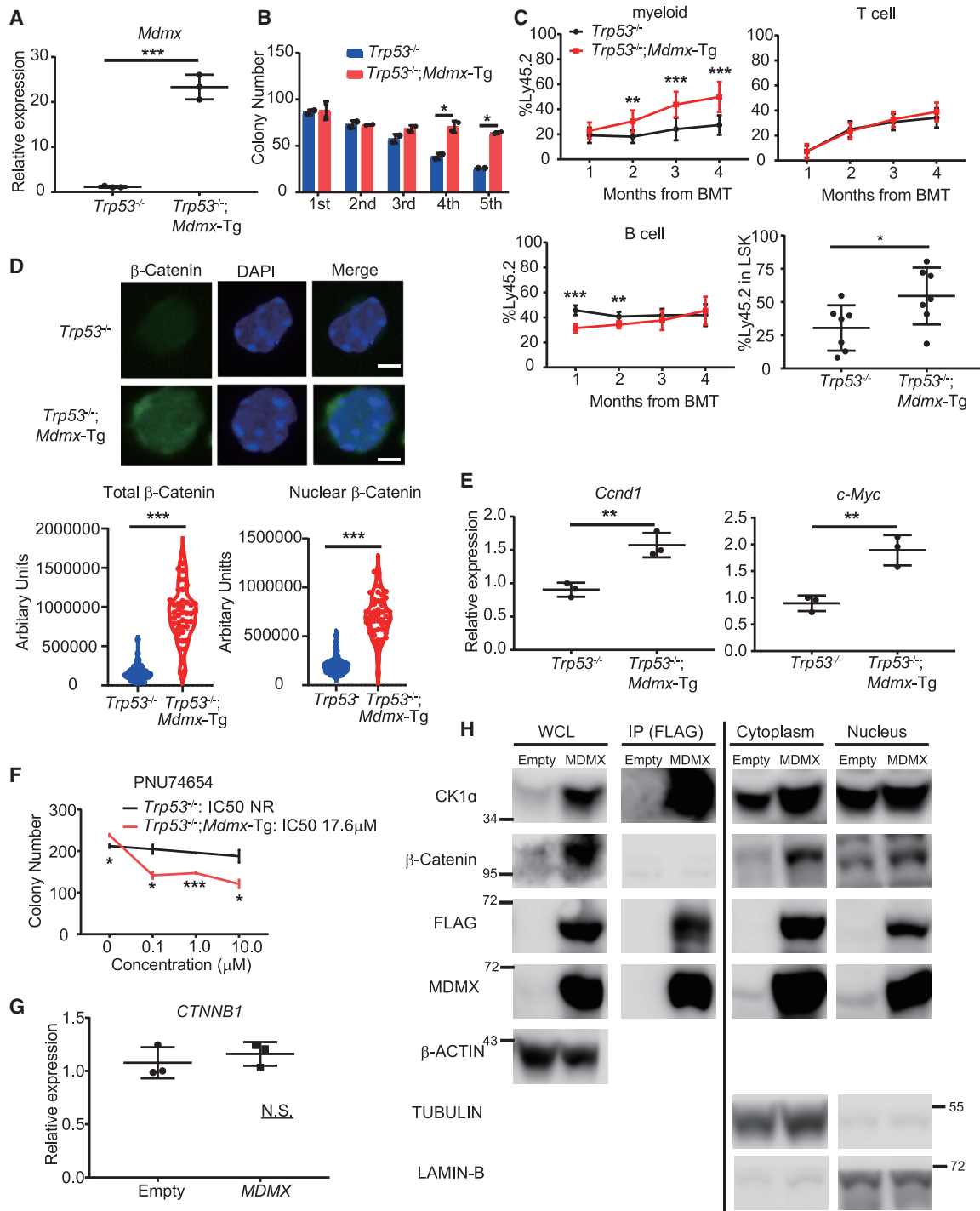


Figure 7. MDMX-driven HSC expansion and Wnt/β-Catenin upregulation is p53 independent

(A) *Mdmx* relative transcript expression in HSCs (Fik2⁻ LSK) (n = 3).

(B) Colony-formation assay from 1×10^4 *Trp53*^{-/-} or *Trp53*^{-/-}; *Mdmx*-Tg BM cells. (n = 2).

(C) 0.5×10^6 *Trp53*^{-/-} or *Trp53*^{-/-}; *Mdmx*-Tg BM cells (Ly45.2) with 2.0×10^6 WT competitors (Ly45.1/2) were competitively transplanted into lethally irradiated recipients (Ly45.1). Ratio of donor cells (Ly45.2) at each time point (months) from transplantation (n = 7) and ratio of donor cells (Ly45.2) in the LSK population at 4 months after transplantation (n = 7).

(legend continued on next page)

data demonstrate a novel mechanism of reduced CK1 α availability caused by MDMX overexpression in hematopoietic cells. Moreover, since we observed upregulation of Wnt/ β -Catenin signaling upon MDMX overexpression even in the absence of p53, we conclude that reduced abundance of CK1 α and subsequent Wnt/ β -Catenin upregulation is a p53-independent, principal mechanism of MDMX.

With regard to potential translational utility of our findings, we found that high levels of MDMX correlated with upregulation of Wnt/ β -Catenin signaling and higher leukemic transformation rate in a large cohort of MDS patients, suggesting relevance of the uncovered mechanisms for human disease. Furthermore, we tested whether Wnt/ β -Catenin can be a therapeutic target in AML and preleukemic disease. Although Wnt/ β -Catenin has been reported to be functionally relevant in LSCs (Wang et al., 2010), and preclinical studies revealed that Wnt/ β -Catenin inhibitors are active against AML *in vitro* and *in vivo* (Fiskus et al., 2015; Li et al., 2014), there have been no published clinical trials on the use of Wnt/ β -Catenin inhibitors/modulators in AML/high-risk MDS (Gruszka et al., 2019). Our data therefore suggest that Wnt/ β -Catenin inhibitors might be particularly effective in MDMX-overexpressing patients, and specifically at the preleukemic stage rather than completely transformed AML, or that they may sensitize preleukemic/leukemic cells to other drugs (Heidel et al., 2012; Jiang et al., 2018b). In this regard, we tested a combination of Wnt/ β -Catenin inhibitor and the clinical drug ALRN-6924, which inhibits the MDMX/TP53 interaction. This combinatorial treatment showed promise in that it revealed significant synergism and led to complete elimination of MDMX-overexpressing pre-LSCs and MDMX/p53 inhibitor-resistant AML cells. As MDMX overexpression is common in AML and we showed overexpression of MDMX and Wnt/ β -Catenin is associated with poor outcome of preleukemic patients, this combination could be a promising therapeutic approach for patients with MDS and AML. Currently, there are no clinical options available for the treatment of preleukemic conditions (e.g., CH in progression) or to specifically prevent leukemic transformation (e.g., of high-risk MDS). Our data suggest that Wnt/ β -Catenin inhibitors in combination with MDMX/p53 inhibitors may offer such a targeted anti-pre-LSC strategy in patients with elevated MDMX and should be considered for further testing.

Overall, our findings highlight an important role of MDMX overexpression in preleukemic-to-acute leukemic progression, and reveal CK1 α /Wnt/ β -Catenin as a therapeutically targetable pathway and as a novel p53-independent non-canonical mechanism of MDMX overexpression. Combinatorial targeting of these pathways may provide a possible approach for precision prevention and cancer interception in the early stages of the pathogenesis of myeloid and possibly other MDMX-driven malignancies

STAR★METHODS

Detailed methods are provided in the online version of this paper and include the following:

- KEY RESOURCES TABLE
- RESOURCE AVAILABILITY
 - Lead contact
 - Materials availability
 - Data and code availability
- EXPERIMENTAL MODEL AND SUBJECT DETAILS
 - Cell lines
 - Animal studies
 - Clinical samples
- METHOD DETAILS
 - Analyses of murine models
 - Flow cytometry (FCM)
 - *In vivo* BrdU assays
 - *In vitro* colony forming assays
 - Competitive transplantation assays
 - Transplantation assay of preleukemic/leukemic BM cells
 - Spectral karyotyping (SKY)
 - RNA sequencing (RNA-seq)
 - Immunofluorescence (IF) staining
 - Western blotting (WB)
 - Immunoprecipitation and mass-spectrometry (IP and LC-MS/MS)
 - Subcellular fractionation
 - Quantitative reverse transcriptase-polymerase chain reaction (qRT-PCR)
 - Cell viability assay (IC50)
 - Plasmid construction
 - Virus production and transduction
- QUANTIFICATION AND STATISTICAL ANALYSIS

SUPPLEMENTAL INFORMATION

Supplemental information can be found online at <https://doi.org/10.1016/j.ccell.2021.02.006>.

ACKNOWLEDGMENTS

We thank M. Dawlaty at the Albert Einstein College of Medicine for sharing FUW-IRES-puro lentiviral vector, K. Gritsman at the Albert Einstein college of Medicine for sharing Phi-Eco retroviral helper vector, R. Levine at Memorial Sloan Kettering Cancer Center for sharing MSCV-NRAS-G12D-IRES-GFP retroviral vector, and S. Martinez-Hoyer at Erasmus Medical Centre and B. Ebert at Dana-Farber Cancer Institute for sharing MSCV-Csnk1a1-IRES-GFP retroviral vector. Expert technical supported was provided by the Stem Cell Isolation and Xenotransplantation Core Facility (funded by NYSTEM grant #C029154) of the Gottesman Institute for Stem Cell and Regenerative

(D) IF staining of β -Catenin (green) with DAPI (blue) in HSC of *Trp53^{-/-}* and *Trp53^{-/-};Mdmx-Tg* mice. Top: representative pictures (scale bars: 1.85 μ m). Bottom: (left) signal of total cell staining of β -Catenin, (right) nuclear signal of β -Catenin with DAPI counterstain.

(E) Relative transcript levels of the β -Catenin target genes *Ccnd1* and *c-Myc*.

(F) Colony number from 1,000 *Trp53^{-/-}* or *Trp53^{-/-};Mdmx-Tg* HSCs with indicated concentration of Wnt/ β -Catenin inhibitor PNU74654 (n = 2).

(G) Relative expression of *CTNNB1* (β -Catenin) RNA in HL-60 cells transduced with *MDMX* or Empty control lentivirus (n = 3).

(H) WCL and cytoplasmic and nuclear extracts from HL-60 cells transduced by FLAG-tagged *MDMX* (*MDMX*) or Empty control lentivirus (Empty). IP for WCL by anti-FLAG beads was performed. WCL, IP, and cytoplasmic and nuclear extract were blotted by indicated antibodies. Molecular weight (kDa) is indicated in the figure. # (A–G) Statistical significance was calculated by t test. Data shown as mean \pm SEM. *0.01 \leq p < 0.05, **0.001 \leq p < 0.01, ***p < 0.001.

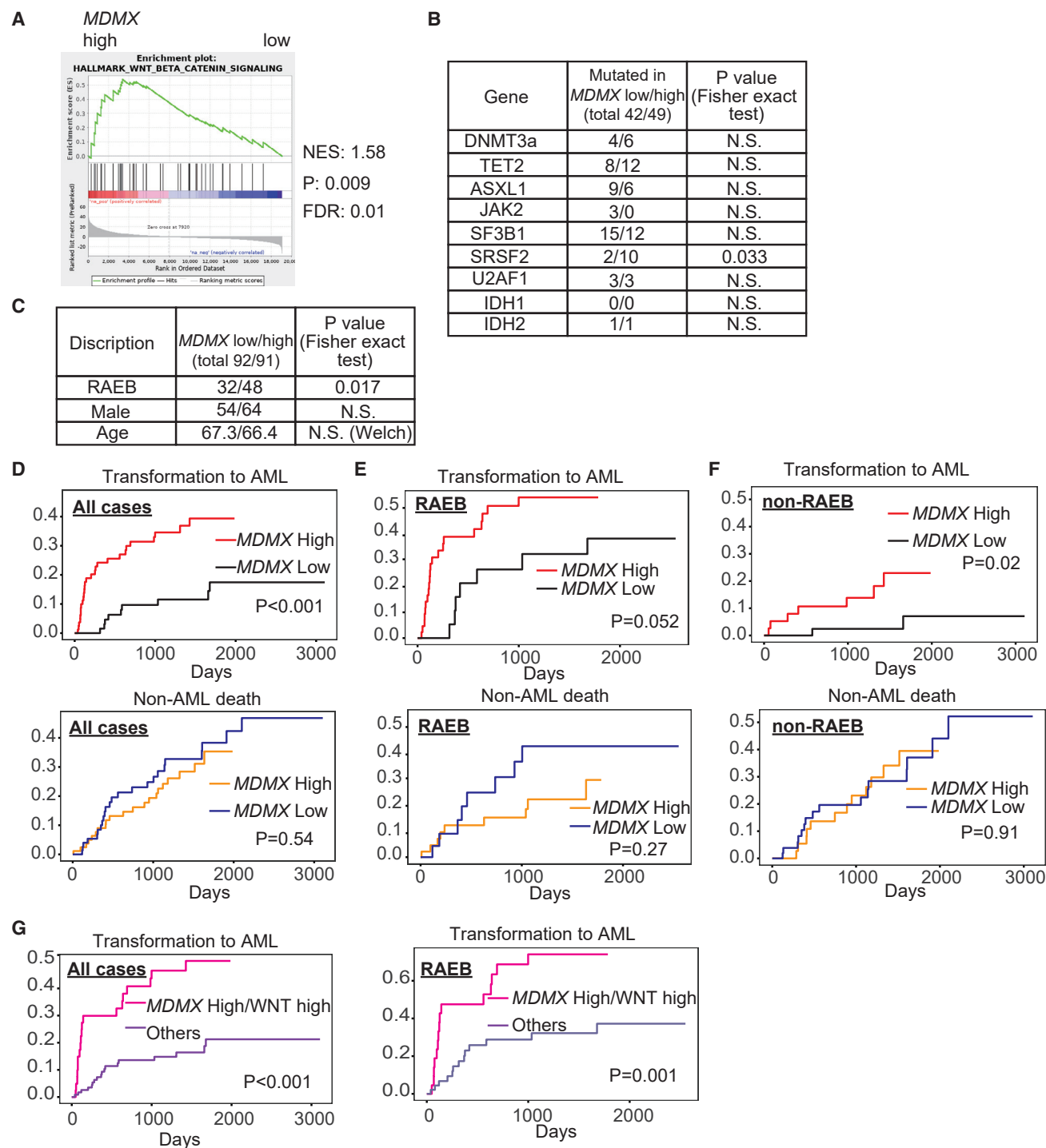


Figure 8. Clinical-correlative data indicate relevance of the *MDMX*-Wnt/ β -Catenin axis in patients with MDS

Analyses of GSE19429.

(A) GSEA of *MDMX*-high versus -low patients reveals highly significant enrichment of Wnt/ β -Catenin signature.

(B) Mutation status of CH related genes between *MDMX*-low and -high patients. p values were calculated by Fisher exact test.

(C) Disease subtype, sex, and age between *MDMX*-low and -high patients. p values were calculated by Fisher exact test for subtype and sex, and Welch's test for age.

(D–F) (D) Cumulative incidence plots of transformation to AML and non-leukemic death treating each other as competing risk (*MDMX* low versus high, all cases), (E) patients with RAEB subtype, and (F) patients with MDS subtypes other than RAEB. p values were calculated by Gray's test.

(G) Cumulative incidence plots of transformation to AML treating non-leukemic death as competing risk (*MDMX* high, WNT score high versus all other cases) (left, all patients; right, patients with RAEB subtype). p values were calculated by Gray's test. See also [Figure S8](#).

Medicine Research, Analytical Imaging Facility (Andrea Briceno) and Genetics core (David Reynolds) of the Albert Einstein College of Medicine. This work was supported by Jane A. and Myles P. Dempsey, NIH grants (U.S., R01CA217092, R01HL150832; A.V., R01HL139487, R01HL150832; G.L., R01CA047296), as well as the Albert Einstein Cancer Center Support Grant (P30CA013330), the Taub Foundation Grants Program for MDS Research (to U.S.), EvansMDS (to U.S. and A.V.), the V Foundation for Cancer Research (to U.S. and A.V.), the Albert Einstein Medical Scientist Training Program (J.C.W. and E.S., T32GM007288), the Albert Einstein Training Program in Stem Cell Biology (T.I.T., NYSTEM #N14I-006), a Ruth L. Kirschstein National Research Service Award (J.C.W., F30GM122308), an NYSCF Druckenmiller fellowship (S.J.T.), Blood Cancer UK (A.P. and J.B., grants 13042 and 19004) and postdoctoral fellowships of the Leukemia & Lymphoma Society (R.K. and S.J.T.). U.S. is the Diane and Arthur B. Belfer Scholar in Cancer Research of the Albert Einstein College of Medicine.

AUTHOR CONTRIBUTIONS

Conceptualization, K.U. and U.S.; methodology, K.U., R.K., C.M., S.X., and G.L.; formal analysis, K.U., R.K., E.S., K.P., B.B., and J.C.; investigation, K.U., R.K., J.C.W., O.B., S.R.N., S.T., L.A.C., T.I.T., H.G., D.S., J.S., Y.S., A.P., and J.B.; writing – original draft, K.U., U.S.; writing – review & editing, R.K., E.S., S.T., C.M., and G.L.; funding acquisition, A.V. and U.S.; supervision, U.S.

DECLARATION OF INTERESTS

L.A.C. is a past employee of Aileron Therapeutics. J.C. is currently an employee of Stelexis Therapeutics. ALRN-6924 was provided to U.S. from Aileron Therapeutics. U.S. has received research funding from GlaxoSmithKline, Bayer HealthCare, Aileron Therapeutics, and Novartis; has received compensation for consultancy services and for serving on scientific advisory boards from GlaxoSmithKline, Bayer Healthcare, Celgene, Aileron Therapeutics, Stelexis Therapeutics, and Pieris Pharmaceuticals; and has equity ownership in and is serving on the board of directors of Stelexis Therapeutics.

Received: May 12, 2020

Revised: November 23, 2020

Accepted: February 8, 2021

Published: March 4, 2021

REFERENCES

Bacher, U., Haferlach, T., Schoch, C., Kern, W., and Schnittger, S. (2006). Implications of NRAS mutations in AML: a study of 2502 patients. *Blood* 107, 3847–3853.

Bereshchenko, O., Mancini, E., Moore, S., Bilbao, D., Mansson, R., Luc, S., Grover, A., Jacobsen, S.E., Bryder, D., and Nerlov, C. (2009). Hematopoietic stem cell expansion precedes the generation of committed myeloid leukemia-initiating cells in C/EBPalpha mutant AML. *Cancer Cell* 16, 390–400.

Bhagat, T.D., Chen, S., Bartenstein, M., Barlowe, A.T., Von Ahrens, D., Choudhary, G.S., Tivnan, P., Amin, E., Marcondes, A.M., Sanders, M.A., et al. (2017). Epigenetically aberrant stroma in MDS propagates disease via Wnt/beta-catenin activation. *Cancer Res.* 77, 4846–4857.

Busque, L., Patel, J.P., Figueroa, M.E., Vasanthakumar, A., Provost, S., Hamilou, Z., Mollica, L., Li, J., Viale, A., Heguy, A., et al. (2012). Recurrent somatic TET2 mutations in normal elderly individuals with clonal hematopoiesis. *Nat. Genet.* 44, 1179–1181.

Cancer Genome Atlas Research Network, Ley, T.J., Miller, C., Ding, L., Raphael, B.J., Mungall, A.J., Robertson, A., Hoadley, K., Triche, T.J., Jr., Laird, P.W., et al. (2013). Genomic and epigenomic landscapes of adult de novo acute myeloid leukemia. *N. Engl. J. Med.* 368, 2059–2074.

Carreras Puigvert, J., Von Stechow, L., Siddappa, R., Pines, A., Bahjat, M., Haazen, L.C., Olsen, J.V., Vrieling, H., Meerman, J.H., Mullenders, L.H., et al. (2013). Systems biology approach identifies the kinase Csnk1a1 as a regulator of the DNA damage response in embryonic stem cells. *Sci. Signal.* 6, ra5.

Carvajal, L.A., Neriah, D.B., Senecal, A., Benard, L., Thiruthuvanathan, V., Yatsenko, T., Narayanagari, S.R., Wheat, J.C., Todorova, T.I., Mitchell, K., et al. (2018). Dual inhibition of MDMX and MDM2 as a therapeutic strategy in leukemia. *Sci. Transl. Med.* 10, eaac3003.

Chen, J., Kao, Y.R., Sun, D., Todorova, T.I., Reynolds, D., Narayanagari, S.R., Montagna, C., Will, B., Verma, A., and Steidl, U. (2019). Myelodysplastic syndrome progression to acute myeloid leukemia at the stem cell level. *Nat. Med.* 25, 103–110.

Chen, L., Li, C., Pan, Y., and Chen, J. (2005). Regulation of p53-MDMX interaction by casein kinase 1 alpha. *Mol. Cell Biol.* 25, 6509–6520.

Chou, T.C. (2006). Theoretical basis, experimental design, and computerized simulation of synergism and antagonism in drug combination studies. *Pharmacol. Rev.* 58, 621–681.

Cobas, M., Wilson, A., Ernst, B., Mancini, S.J., Macdonald, H.R., Kemler, R., and Radtke, F. (2004). Beta-catenin is dispensable for hematopoiesis and lymphopoiesis. *J. Exp. Med.* 199, 221–229.

Dewaele, M., Tabaglio, T., Willekens, K., Bezzi, M., Teo, S.X., Low, D.H., Koh, C.M., Rambow, F., Fiers, M., Rogiers, A., et al. (2016). Antisense oligonucleotide-mediated MDM4 exon 6 skipping impairs tumor growth. *J. Clin. Invest.* 126, 68–84.

Dumble, M., Moore, L., Chambers, S.M., Geiger, H., Van Zant, G., Goodell, M.A., and Donehower, L.A. (2007). The impact of altered p53 dosage on hematopoietic stem cell dynamics during aging. *Blood* 109, 1736–1742.

Fenaux, P., Preudhomme, C., Quiquandon, I., Jonveaux, P., Lai, J.L., Vanrumbeke, M., Loucheux-Lefebvre, M.H., Bauters, F., Berger, R., and Kerckaert, J.P. (1992). Mutations of the P53 gene in acute myeloid leukaemia. *Br. J. Haematol.* 80, 178–183.

Fiskus, W., Sharma, S., Saha, S., Shah, B., Devaraj, S.G., Sun, B., Horrigan, S., Leveque, C., Zu, Y., Iyer, S., et al. (2015). Pre-clinical efficacy of combined therapy with novel beta-catenin antagonist BC2059 and histone deacetylase inhibitor against AML cells. *Leukemia* 29, 1267–1278.

Genovese, G., Kahler, A.K., Handsaker, R.E., Lindberg, J., Rose, S.A., Bakhoum, S.F., Chambert, K., Mick, E., Neale, B.M., Fromer, M., et al. (2014). Clonal hematopoiesis and blood-cancer risk inferred from blood DNA sequence. *N. Engl. J. Med.* 371, 2477–2487.

Gilliland, D.G., and Tallman, M.S. (2002). Focus on acute leukemias. *Cancer Cell* 1, 417–420.

Gruszka, A.M., Valli, D., and Alcalay, M. (2019). Wnt signalling in acute myeloid leukaemia. *Cells* 8, 1403.

Han, X., Medeiros, L.J., Zhang, Y.H., You, M.J., Andreeff, M., Konopleva, M., and Bueso-Ramos, C.E. (2016). High expression of human homologue of murine double minute 4 and the short splicing variant, HDM4-S, in bone marrow in patients with acute myeloid leukemia or myelodysplastic syndrome. *Clin. Lymphoma Myeloma Leuk.* 16 (Suppl), S30–S38.

Heidel, F.H., Bullinger, L., Feng, Z., Wang, Z., Neff, T.A., Stein, L., Kalaitzidis, D., Lane, S.W., and Armstrong, S.A. (2012). Genetic and pharmacologic inhibition of beta-catenin targets imatinib-resistant leukemia stem cells in CML. *Cell Stem Cell* 10, 412–424.

Hou, H.A., Chou, W.C., Kuo, Y.Y., Liu, C.Y., Lin, L.I., Tseng, M.H., Chiang, Y.C., Liu, M.C., Liu, C.W., Tang, J.L., et al. (2015). TP53 mutations in de novo acute myeloid leukemia patients: longitudinal follow-ups show the mutation is stable during disease evolution. *Blood Cancer J.* 5, e331.

Ito, K., Lee, J., Chrysanthou, S., Zhao, Y., Josephs, K., Sato, H., Teruya-Feldstein, J., Zheng, D., Dawlaty, M.M., and Ito, K. (2019). Non-catalytic roles of Tet2 are essential to regulate hematopoietic stem and progenitor cell homeostasis. *Cell Rep.* 28, 2480–2490.e4.

Jaiswal, S., Fontanillas, P., Flannick, J., Manning, A., Grauman, P.V., Mar, B.G., Lindsley, R.C., Mermel, C.H., Burt, N., Chavez, A., et al. (2014). Age-related clonal hematopoiesis associated with adverse outcomes. *N. Engl. J. Med.* 371, 2488–2498.

Jan, M., Snyder, T.M., Corces-Zimmerman, M.R., Vyas, P., Weissman, I.L., Quake, S.R., and Majeti, R. (2012). Clonal evolution of preleukemic hematopoietic stem cells precedes human acute myeloid leukemia. *Sci. Transl. Med.* 4, 149ra118.

- Jaras, M., Miller, P.G., Chu, L.P., Puram, R.V., Fink, E.C., Schneider, R.K., Al-Shahrour, F., Pena, P., Breyfogle, L.J., Hartwell, K.A., et al. (2014). Csnk1a1 inhibition has p53-dependent therapeutic efficacy in acute myeloid leukemia. *J. Exp. Med.* *211*, 605–612.
- Jiang, S., Zhang, M., Sun, J., and Yang, X. (2018a). Casein kinase 1alpha: biological mechanisms and theranostic potential. *Cell Commun. Signal.* *16*, 23.
- Jiang, X., Mak, P.Y., Mu, H., Tao, W., Mak, D.H., Kornblau, S., Zhang, Q., Ruvolo, P., Burks, J.K., Zhang, W., et al. (2018b). Disruption of Wnt/beta-catenin exerts antileukemia activity and synergizes with FLT3 inhibition in FLT3-mutant acute myeloid leukemia. *Clin. Cancer Res.* *24*, 2417–2429.
- Kadia, T.M., Jain, P., Ravandi, F., Garcia-Manero, G., Andreef, M., Takahashi, K., Borthakur, G., Jabbour, E., Konopleva, M., Daver, N.G., et al. (2016). TP53 mutations in newly diagnosed acute myeloid leukemia: clinicomolecular characteristics, response to therapy, and outcomes. *Cancer* *122*, 3484–3491.
- Kandoth, C., McLellan, M.D., Vandin, F., Ye, K., Niu, B., Lu, C., Xie, M., Zhang, Q., McMichael, J.F., Wyczalkowski, M.A., et al. (2013). Mutational landscape and significance across 12 major cancer types. *Nature* *502*, 333–339.
- Kawahara, M., Pandolfi, A., Bartholdy, B., Barreiro, L., Will, B., Roth, M., Okoye-Okafor, U.C., Todorova, T.I., Figueroa, M.E., Melnick, A., et al. (2012). H2O-like homeobox regulates early hematopoiesis and promotes acute myeloid leukemia. *Cancer Cell* *22*, 194–208.
- Kiyoi, H., Naoe, T., Nakano, Y., Yokota, S., Minami, S., Miyawaki, S., Asou, N., Kuriyama, K., Jinnai, I., Shimazaki, C., et al. (1999). Prognostic implication of FLT3 and N-RAS gene mutations in acute myeloid leukemia. *Blood* *93*, 3074–3080.
- Ko, M., Bandukwala, H.S., An, J., Lamperti, E.D., Thompson, E.C., Hastie, R., Tsangaratos, A., Rajewsky, K., Korolov, S.B., and Rao, A. (2011). Ten-Eleven-Translocation 2 (TET2) negatively regulates homeostasis and differentiation of hematopoietic stem cells in mice. *Proc. Natl. Acad. Sci. U S A* *108*, 14566–14571.
- Kondo, M., Weissman, I.L., and Akashi, K. (1997). Identification of clonogenic common lymphoid progenitors in mouse bone marrow. *Cell* *91*, 661–672.
- Kuo, Y.H., Landrette, S.F., Heilman, S.A., Perratt, P.N., Garrett, L., Liu, P.P., Le Beau, M.M., Kogan, S.C., and Castilla, L.H. (2006). Cbf beta-SMMHC induces distinct abnormal myeloid progenitors able to develop acute myeloid leukemia. *Cancer Cell* *9*, 57–68.
- Lavallee, V.P., Bacceilli, I., Krosi, J., Wilhelm, B., Barabe, F., Gendron, P., Boucher, G., Lemieux, S., Marinier, A., Meloche, S., et al. (2015). The transcriptomic landscape and directed chemical interrogation of MLL-rearranged acute myeloid leukemias. *Nat. Genet.* *47*, 1030–1037.
- Lee, B.H., Tothova, Z., Levine, R.L., Anderson, K., Buza-Vidas, N., Cullen, D.E., McDowell, E.P., Adelsperger, J., Frohling, S., Huntly, B.J., et al. (2007). FLT3 mutations confer enhanced proliferation and survival properties to multipotent progenitors in a murine model of chronic myelomonocytic leukemia. *Cancer Cell* *12*, 367–380.
- Li, B., Orton, D., Neitzel, L.R., Astudillo, L., Shen, C., Long, J., Chen, X., Kirkbride, K.C., Doundoulakis, T., Guerra, M.L., et al. (2017). Differential abundance of CK1alpha provides selectivity for pharmacological CK1alpha activators to target WNT-dependent tumors. *Sci. Signal.* *10*, eaak9916.
- Li, K., Hu, C., Mei, C., Ren, Z., Vera, J.C., Zhuang, Z., Jin, J., and Tong, H. (2014). Sequential combination of decitabine and idarubicin synergistically enhances anti-leukemia effect followed by demethylating Wnt pathway inhibitor promoters and downregulating Wnt pathway nuclear target. *J. Transl. Med.* *12*, 167.
- Li, S., Garrett-Bakelman, F.E., Chung, S.S., Sanders, M.A., Hricik, T., Rapaport, F., Patel, J., Dillon, R., Vijay, P., Brown, A.L., et al. (2016). Distinct evolution and dynamics of epigenetic and genetic heterogeneity in acute myeloid leukemia. *Nat. Med.* *22*, 792–799.
- Liu, C., Li, Y., Semenov, M., Han, C., Baeg, G.H., Tan, Y., Zhang, Z., Lin, X., and He, X. (2002). Control of beta-catenin phosphorylation/degradation by a dual-kinase mechanism. *Cell* *108*, 837–847.
- Liu, J., Pan, S., Hsieh, M.H., Ng, N., Sun, F., Wang, T., Kasibhatla, S., Schuller, A.G., Li, A.G., Cheng, D., et al. (2013). Targeting Wnt-driven cancer through the inhibition of porcupine by LGK974. *Proc. Natl. Acad. Sci. U S A* *110*, 20224–20229.
- Liu, Y., Elf, S.E., Miyata, Y., Sashida, G., Liu, Y., Huang, G., Di Giandomenico, S., Lee, J.M., Deblasio, A., Menendez, S., et al. (2009). p53 regulates hematopoietic stem cell quiescence. *Cell Stem Cell* *4*, 37–48.
- Love, M.I., Huber, W., and Anders, S. (2014). Moderated estimation of fold change and dispersion for RNA-seq data with DESeq2. *Genome Biol.* *15*, 550.
- Mayle, A., Luo, M., Jeong, M., and Goodell, M.A. (2013). Flow cytometry analysis of murine hematopoietic stem cells. *Cytometry A* *83*, 27–37.
- Mizuki, M., Schwable, J., Steur, C., Choudhary, C., Agrawal, S., Sargin, B., Steffen, B., Matsumura, I., Kanakura, Y., Bohmer, F.D., et al. (2003). Suppression of myeloid transcription factors and induction of STAT response genes by AML-specific Flt3 mutations. *Blood* *101*, 3164–3173.
- Montagna, C., Lyu, M.S., Hunter, K., Lukes, L., Lowther, W., Reppert, T., Hissong, B., Weaver, Z., and Ried, T. (2003). The Septin 9 (MSF) gene is amplified and overexpressed in mouse mammary gland adenocarcinomas and human breast cancer cell lines. *Cancer Res.* *63*, 2179–2187.
- Moran-Crusio, K., Reavie, L., Shih, A., Abdel-Wahab, O., Ndiaye-Lobry, D., Lobry, C., Figueroa, M.E., Vasanthakumar, A., Patel, J., Zhao, X., et al. (2011). Tet2 loss leads to increased hematopoietic stem cell self-renewal and myeloid transformation. *Cancer Cell* *20*, 11–24.
- Muller, P.A., and Vousden, K.H. (2013). p53 mutations in cancer. *Nat. Cell Biol.* *15*, 2–8.
- Nabbi, A., and Riabowol, K. (2015). Rapid isolation of nuclei from cells in vitro. *Cold Spring Harb. Protoc.* *2015*, 769–772.
- Nakao, M., Yokota, S., Iwai, T., Kaneko, H., Horiike, S., Kashima, K., Sonoda, Y., Fujimoto, T., and Misawa, S. (1996). Internal tandem duplication of the flt3 gene found in acute myeloid leukemia. *Leukemia* *10*, 1911–1918.
- Padilla-Nash, H.M., Barenboim-Stapleton, L., Difilippantonio, M.J., and Ried, T. (2006). Spectral karyotyping analysis of human and mouse chromosomes. *Nat. Protoc.* *1*, 3129–3142.
- Papaemmanuil, E., Dohner, H., and Campbell, P.J. (2016). Genomic classification in acute myeloid leukemia. *N. Engl. J. Med.* *375*, 900–901.
- Parikh, C., Subrahmanyam, R., and Ren, R. (2007). Oncogenic NRAS, KRAS, and HRAS exhibit different leukemogenic potentials in mice. *Cancer Res.* *67*, 7139–7146.
- Patro, R., Duggal, G., Love, M.I., Irizarry, R.A., and Kingsford, C. (2017). Salmon provides fast and bias-aware quantification of transcript expression. *Nat. Methods* *14*, 417–419.
- Peller, S., and Rotter, V. (2003). TP53 in hematological cancer: low incidence of mutations with significant clinical relevance. *Hum. Mutat.* *21*, 277–284.
- Pietras, E.M., Reynaud, D., Kang, Y.A., Carlin, D., Calero-Nieto, F.J., Leavitt, A.D., Stuart, J.M., Gottgens, B., and Passegue, E. (2015). Functionally distinct subsets of lineage-biased multipotent progenitors control blood production in normal and regenerative conditions. *Cell Stem Cell* *17*, 35–46.
- Quintas-Cardama, A., Hu, C., Qutub, A., Qiu, Y.H., Zhang, X., Post, S.M., Zhang, N., Coombes, K., and Kornblau, S.M. (2017). p53 pathway dysfunction is highly prevalent in acute myeloid leukemia independent of TP53 mutational status. *Leukemia* *31*, 1296–1305.
- Reed, S.E., Staley, E.M., Mayginnes, J.P., Pintel, D.J., and Tullis, G.E. (2006). Transfection of mammalian cells using linear polyethylenimine is a simple and effective means of producing recombinant adeno-associated virus vectors. *J. Virol. Methods* *138*, 85–98.
- Rosenbauer, F., Wagner, K., Kutok, J.L., Iwasaki, H., Le Beau, M.M., Okuno, Y., Akashi, K., Fiering, S., and Tenen, D.G. (2004). Acute myeloid leukemia induced by graded reduction of a lineage-specific transcription factor, PU.1. *Nat. Genet.* *36*, 624–630.
- Sallman, D.A., Borate, U., Cull, E.H., Donnellan, W.B., Komrokji, R.S., Steidl, U., Corvez, M.M., Payton, M., Annis, D.A., Pinchasik, D., et al. (2018). Phase 1/1b study of the stapled peptide ALRN-6924, a dual inhibitor of MDMX and MDM2, as monotherapy or in combination with cytarabine for the treatment of relapsed/refractory AML and advanced MDS with TP53 wild-type. *Blood (meeting abstract)* *132 (Supplement 1)*, 4066.

- Scheller, M., Huelsken, J., Rosenbauer, F., Taketo, M.M., Birchmeier, W., Tenen, D.G., and Leutz, A. (2006). Hematopoietic stem cell and multilineage defects generated by constitutive beta-catenin activation. *Nat. Immunol.* **7**, 1037–1047.
- Shlush, L.I., Mitchell, A., Heisler, L., Abelson, S., Ng, S.W.K., Trotman-Grant, A., Medeiros, J.J.F., Rao-Bhatia, A., Jaciw-Zurakowsky, I., Marke, R., et al. (2017). Tracing the origins of relapse in acute myeloid leukaemia to stem cells. *Nature* **547**, 104–108.
- Shlush, L.I., Zandi, S., Mitchell, A., Chen, W.C., Brandwein, J.M., Gupta, V., Kennedy, J.A., Schimmer, A.D., Schuh, A.C., Yee, K.W., et al. (2014). Identification of pre-leukaemic haematopoietic stem cells in acute leukaemia. *Nature* **506**, 328–333.
- Sive, J.I., Basilico, S., Hannah, R., Kinston, S.J., Calero-Nieto, F.J., and Gottgens, B. (2016). Genome-scale definition of the transcriptional programme associated with compromised PU.1 activity in acute myeloid leukaemia. *Leukemia* **30**, 14–23.
- Staber, P.B., Zhang, P., Ye, M., Welner, R.S., Levantini, E., Di Ruscio, A., Ebraldize, A.K., Bach, C., Zhang, H., Zhang, J., et al. (2014). The Runx-PU.1 pathway preserves normal and AML/ETO9a leukemic stem cells. *Blood* **124**, 2391–2399.
- Steidl, U., Rosenbauer, F., Verhaak, R.G., Gu, X., Ebraldize, A., Otu, H.H., Klippel, S., Steidl, C., Bruns, I., Costa, D.B., et al. (2006). Essential role of Jun family transcription factors in PU.1 knockdown-induced leukemic stem cells. *Nat. Genet.* **38**, 1269–1277.
- Steidl, U., Steidl, C., Ebraldize, A., Chapuy, B., Han, H.J., Will, B., Rosenbauer, F., Becker, A., Wagner, K., Koschmieder, S., et al. (2007). A distal single nucleotide polymorphism alters long-range regulation of the PU.1 gene in acute myeloid leukemia. *J. Clin. Invest.* **117**, 2611–2620.
- Subramanian, A., Tamayo, P., Mootha, V.K., Mukherjee, S., Ebert, B.L., Gillette, M.A., Paulovich, A., Pomeroy, S.L., Golub, T.R., Lander, E.S., et al. (2005). Gene set enrichment analysis: a knowledge-based approach for interpreting genome-wide expression profiles. *Proc. Natl. Acad. Sci. U S A* **102**, 15545–15550.
- Tenen, D.G. (2003). Disruption of differentiation in human cancer: AML shows the way. *Nat. Rev. Cancer* **3**, 89–101.
- Tremblay, M., Tremblay, C.S., Herblot, S., Aplan, P.D., Hebert, J., Perreault, C., and Hoang, T. (2010). Modeling T-cell acute lymphoblastic leukemia induced by the SCL and LMO1 oncogenes. *Genes Dev.* **24**, 1093–1105.
- Trosset, J.Y., Dalvit, C., Knapp, S., Fasolini, M., Veronesi, M., Mantegani, S., Gianellini, L.M., Catana, C., Sundstrom, M., Stouten, P.F., et al. (2006). Inhibition of protein-protein interactions: the discovery of druglike beta-catenin inhibitors by combining virtual and biophysical screening. *Proteins* **64**, 60–67.
- Vangala, R.K., Heiss-Neumann, M.S., Rangatia, J.S., Singh, S.M., Schoch, C., Tenen, D.G., Hiddemann, W., and Behre, G. (2003). The myeloid master regulator transcription factor PU.1 is inactivated by AML1-ETO in t(8;21) myeloid leukemia. *Blood* **101**, 270–277.
- Wade, M., Li, Y.C., and Wahl, G.M. (2013). MDM2, MDMX and p53 in oncogenesis and cancer therapy. *Nat. Rev. Cancer* **13**, 83–96.
- Wang, Y., Krivtsov, A.V., Sinha, A.U., North, T.E., Goessling, W., Feng, Z., Zon, L.I., and Armstrong, S.A. (2010). The Wnt/beta-catenin pathway is required for the development of leukemia stem cells in AML. *Science* **327**, 1650–1653.
- Will, B., Vogler, T.O., Narayanagari, S., Bartholdy, B., Todorova, T.I., Da Silva Ferreira, M., Chen, J., Yu, Y., Mayer, J., Barreyro, L., et al. (2015). Minimal PU.1 reduction induces a preleukemic state and promotes development of acute myeloid leukemia. *Nat. Med.* **21**, 1172–1181.
- Will, B., Zhou, L., Vogler, T.O., Ben-Neriah, S., Schinke, C., Tamari, R., Yu, Y., Bhagat, T.D., Bhattacharyya, S., Barreyro, L., et al. (2012). Stem and progenitor cells in myelodysplastic syndromes show aberrant stage-specific expansion and harbor genetic and epigenetic alterations. *Blood* **120**, 2076–2086.
- Wu, S., Chen, L., Becker, A., Schonbrunn, E., and Chen, J. (2012). Casein kinase 1alpha regulates an MDMX intramolecular interaction to stimulate p53 binding. *Mol. Cell Biol.* **32**, 4821–4832.
- Xie, M., Lu, C., Wang, J., McLellan, M.D., Johnson, K.J., Wendl, M.C., McMichael, J.F., Schmidt, H.K., Yellapantula, V., Miller, C.A., et al. (2014). Age-related mutations associated with clonal hematopoietic expansion and malignancies. *Nat. Med.* **20**, 1472–1478.
- Xiong, S., Pant, V., Suh, Y.A., Van Pelt, C.S., Wang, Y., Valentin-Vega, Y.A., Post, S.M., and Lozano, G. (2010). Spontaneous tumorigenesis in mice overexpressing the p53-negative regulator Mdm4. *Cancer Res.* **70**, 7148–7154.
- Xiong, S., Pant, V., Zhang, Y., Aryal, N.K., You, M.J., Kusewitt, D., and Lozano, G. (2017). The p53 inhibitor Mdm4 cooperates with multiple genetic lesions in tumorigenesis. *J. Pathol.* **241**, 501–510.
- Xu, Y., Lin, Z., Tang, C., Tang, Y., Cai, Y., Zhong, H., Wang, X., Zhang, W., Xu, C., Wang, J., et al. (2019). A new massively parallel nanoball sequencing platform for whole exome research. *BMC Bioinformatics* **20**, 153.
- Yoshida, H., Ichikawa, H., Tagata, Y., Katsumoto, T., Ohnishi, K., Akao, Y., Naoe, T., Pandolfi, P.P., and Kitabayashi, I. (2007). PML-retinoic acid receptor alpha inhibits PML IV enhancement of PU.1-induced C/EBPepsilon expression in myeloid differentiation. *Mol. Cell Biol.* **27**, 5819–5834.
- Zeisig, B.B., Kulasekararaj, A.G., Mufti, G.J., and So, C.W. (2012). SnapShot: acute myeloid leukemia. *Cancer Cell* **22**, 698–698.e1.
- Zhan, T., Rindtorff, N., and Boutros, M. (2017). Wnt signaling in cancer. *Oncogene* **36**, 1461–1473.
- Zhang, J., Kong, G., Rajagopalan, A., Lu, L., Song, J., Hussaini, M., Zhang, X., Ranheim, E.A., Liu, Y., Wang, J., et al. (2017). p53^{-/-} synergizes with enhanced NrasG12D signaling to transform megakaryocyte-erythroid progenitors in acute myeloid leukemia. *Blood* **129**, 358–370.
- Zhu, F.Y., Chen, M.X., Ye, N.H., Qiao, W.M., Gao, B., Law, W.K., Tian, Y., Zhang, D., Zhang, D., Liu, T.Y., et al. (2018). Comparative performance of the BGISEQ-500 and Illumina HiSeq4000 sequencing platforms for transcriptome analysis in plants. *Plant Methods* **14**, 69.

STAR★METHODS

KEY RESOURCES TABLE

REAGENT or RESOURCE	SOURCE	IDENTIFIER
Antibodies		
Mouse Anti-Human CD2 (PE/Cyamine5)	Thermo Fisher Scientific	Cat# 15-0029-73, RRID:AB_468687
Mouse Anti-Human CD3 (PE/Cyamine5)	Thermo Fisher Scientific	Cat# 15-0038-42, RRID:AB_10598354
Mouse Anti-Human CD4 (Tri-Color)	Thermo Fisher Scientific	Cat# MHCD0406, RRID:AB_1473737
Mouse Anti-Human CD7 (Tri-Color)	Thermo Fisher Scientific	Cat# MHCD0706, RRID:AB_1482844
Mouse Anti-Human CD8 (Tri-Color)	Thermo Fisher Scientific	Cat# MHCD0806, RRID:AB_10372207
Mouse Anti-Human CD10 (PE/Cyamine5)	Thermo Fisher Scientific	Cat# 15-0106-73, RRID:AB_657520
Mouse Anti-Human CD14 (Tri-Color)	Thermo Fisher Scientific	Cat# MHCD1406, RRID:AB_10373566
Mouse Anti-Human CD19 (PE/Cyamine5)	Thermo Fisher Scientific	Cat# 15-0199-42, RRID:AB_10853658
Mouse Anti-Human CD20 (PE/Cyamine5)	Thermo Fisher Scientific	Cat# 15-0209-42, RRID:AB_10548510
Mouse Anti-Human CD235a (PE/Cyamine5)	BD Biosciences	Cat# 559944, RRID:AB_397387
Mouse Anti-Human CD56 (Tri-Color)	Thermo Fisher Scientific	Cat# MHCD5606, RRID:AB_10372520
Mouse Anti-Human CD33 (APC)	Thermo Fisher Scientific	Cat# A15727, RRID:AB_2534507
Mouse Anti-Human CD34 (Pacific Blue)	BioLegend	Cat# 343512, RRID:AB_1877197
Rat Anti-Mouse CD3e (Biotin)	Thermo Fisher Scientific	Cat# 13-0032-82, RRID:AB_2572762
Rat Anti-Mouse CD3e (eFluor450)	Thermo Fisher Scientific	Cat# 48-0031-82, RRID:AB_10735092
Rat Anti-Mouse CD4 (Biotin)	Thermo Fisher Scientific	Cat# 13-0041-82, RRID:AB_466325
Rat Anti-Mouse CD4 (eFluor450)	Thermo Fisher Scientific	Cat# 48-0041-82, RRID:AB_10718983
Rat Anti-Mouse CD4 (PE-Cyamine7)	Thermo Fisher Scientific	Cat# 25-0041-82, RRID:AB_469576
Rat Anti-Mouse CD8a (Biotin)	Thermo Fisher Scientific	Cat# 13-0081-82, RRID:AB_466346
Rat Anti-Mouse CD8a (eFluor450)	Thermo Fisher Scientific	Cat# 48-0081-82, RRID:AB_1272198
Rat Anti-Mouse CD8a (PE-Cyamine7)	Thermo Fisher Scientific	Cat# 25-0081-82, RRID:AB_469584
Rat Anti-Mouse CD11b (APC-eFluor780)	Thermo Fisher Scientific	Cat# 47-0112-82, RRID:AB_1603193
Rat Anti-Mouse CD11b (Biotin)	Thermo Fisher Scientific	Cat# 13-0112-82, RRID:AB_466359
Rat Anti-Mouse CD11b (eFluor450)	Thermo Fisher Scientific	Cat# 48-0112-82, RRID:AB_1582236
Rat Anti-Mouse CD11b (PE)	Thermo Fisher Scientific	Cat# 12-0112-83, RRID:AB_2734870
Rat Anti-Mouse CD16/32 (PE/Cyamine7)	Thermo Fisher Scientific	Cat# 25-0161-82, RRID:AB_469598
Rat Anti-Mouse CD16/32 TruStain fcX (Blocking-Ab)	BioLegend	Cat# 101320, RRID:AB_1574975
Rat Anti-Mouse CD19 (Biotin)	Thermo Fisher Scientific	Cat# 13-0193-82, RRID:AB_657656
Rat Anti-Mouse CD19 (eFluor450)	Thermo Fisher Scientific	Cat# 48-0193-82, RRID:AB_2734905
Rat Anti-Mouse CD25 (eFluor450)	BD Biosciences	Cat# 553866, RRID:AB_395101
Rat Anti-Mouse CD34 (eFluor450)	Thermo Fisher Scientific	Cat# 48-0341-82, RRID:AB_2043837
Rat Anti-Mouse CD34 (FITC)	Thermo Fisher Scientific	Cat# 11-0341-82, RRID:AB_465021
Rat Anti-Human/Mouse CD44 (eFluor450)	Thermo Fisher Scientific	Cat# 48-0441-82, RRID:AB_1272246
Rat Anti-Human/Mouse CD45.1 (FITC)	Thermo Fisher Scientific	Cat# 11-0453-82, RRID:AB_465058
Rat Anti-Human/Mouse CD45.2 (APC-Cyamine7)	Thermo Fisher Scientific	Cat# 47-0454-82, RRID:AB_1272175
Rat Anti-Human/Mouse CD45.2 (PE)	Thermo Fisher Scientific	Cat# 12-0454-82, RRID:AB_465678
Rat Anti-Human/Mouse CD45R (B220) (Biotin)	Thermo Fisher Scientific	Cat# 13-0452-82, RRID:AB_466449
Rat Anti-Human/Mouse CD45R (B220) (eFluor450)	Thermo Fisher Scientific	Cat# 48-0452-82, RRID:AB_1548761
Rat Anti-Mouse CD48 (Alexa-Fluor488)	BioLegend	Cat# 103414, RRID:AB_571979
Rat Anti-Mouse CD48 (PE)	BioLegend	Cat# 103405, RRID:AB_313020

(Continued on next page)

Continued

REAGENT or RESOURCE	SOURCE	IDENTIFIER
Rat Anti-Mouse cKit (CD117) (APC)	Thermo Fisher Scientific	Cat# 17-1171-82, RRID:AB_469430
Rat Anti-Mouse CD127 (Biotin)	Thermo Fisher Scientific	Cat# 13-1271-82, RRID:AB_466588
Rat Anti-Mouse CD127 (eFluor450)	Thermo Fisher Scientific	Cat# 48-1271-82, RRID:AB_2016698
Rat Anti-Mouse CD135 (Flt3/Flk2) (PE)	Thermo Fisher Scientific	Cat# 12-1351-82, RRID:AB_465859
Rat Anti-Mouse CD150 (PE-Cyaminate7)	BioLegend	Cat# 115914, RRID:AB_439797
Rat Anti-Mouse F4/80 (eFluor450)	Thermo Fisher Scientific	Cat# 48-4801-82, RRID:AB_1548747
Rat Anti-Mouse Ly-6A/E (Sca-1) (APC-Cyaminate7)	BD Biosciences	Cat# 560654, RRID:AB_1727552
Rat Anti-Mouse Ly-6G (Gr-1) (Biotin)	Thermo Fisher Scientific	Cat# 13-5931-82, RRID:AB_466800
Rat Anti-Mouse Ly-6G (Gr-1) (eFluor450)	Thermo Fisher Scientific	Cat# 48-5931-82, RRID:AB_1548788
Rat Anti-Mouse Ly-6G (Gr-1) (PE)	Thermo Fisher Scientific	Cat# 12-5931-81, RRID:AB_466044
Rat Anti-Mouse-Ter119 (Biotin)	Thermo Fisher Scientific	Cat# 13-5921-82, RRID:AB_466797
Rat Anti-Mouse-Ter119 (eFluor450)	Thermo Fisher Scientific	Cat# 48-5921-82, RRID:AB_1518808
Streptavidin eFluor450	Thermo Fisher Scientific	Cat# 48-4317-82, RRID:AB_10359737
Streptavidin Pacific Orange	Thermo Fisher Scientific	Cat# S32365
Streptavidin PE-Cyaminate7	Thermo Fisher Scientific	Cat# 25-4317-82, RRID:AB_10116480
Rabbit Anti-Actin (polyclonal)	Sigma Aldrich	Cat# A2066, RRID:AB_476693
Rabbit Anti- β -Catenin (CAT-15) (polyclonal)	Thermo Fisher Scientific	Cat# 71-2700, RRID:AB_2533982
Rabbit Anti- β -Catenin (D10A8) (monoclonal)	Cell Signaling Technology	Cat# 8480 RRID:AB_11127855
Rabbit Anti- β -Tubulin (polyclonal)	Cell Signaling Technology	Cat# 2146, RRID:AB_2210545
Rabbit Anti-CK1 α (EPR1961(2)) (monoclonal)	Abcam	Cat# ab108296, RRID:AB_10864123
Rabbit Anti-FLAG(DYKDDDDK)-Tag (polyclonal)	Cell Signaling Technology	Cat# 2368, RRID:AB_2217020
Rabbit Anti-HA-Tag (C29F4) (monoclonal)	Cell Signaling Technology	Cat# 3724, RRID:AB_1549585
Rabbit Anti-LaminB1 (polyclonal)	Abcam	Cat# ab16048, RRID:AB_443298
Mouse Anti-MDMX (MDMX_82) (monoclonal)	Abcam	Cat# ab49993, RRID:AB_880928
Rabbit Anti-phospho- β -Catenin (Thr41/Ser45) (polyclonal)	Cell Signaling Technology	Cat# 9565, RRID:AB_331731
Horse Anti-Mouse-IgG, HRP-linked (secondary antibody)	Cell Signaling Technology	Cat# 7076, RRID:AB_330924
Horse Anti-Rabbit-IgG, HRP-linked (secondary antibody)	Cell Signaling Technology	Cat# 7074, RRID:AB_2099233
Goat Anti-Rabbit-IgG, Alexa Fluor 488 conjugated	Abcam	Cat# ab150077, RRID:AB_2630356
Mouse TrueBlot ULTRA: Anti-Mouse Ig HRP (secondary antibody)	Rockland	Cat# 18-8817-30, RRID:AB_2610849
Bacterial and virus strains		
FUW-IRES-GFP lentiviral vector	(Ito et al., 2019)	N/A
MSCV-IRES-GFP retroviral vector (MIG)	Addgene	20672
PAX2 (lentiviral helper)	Addgene	35002
pCAD-IRES-GFP lentiviral vector	(Kawahara et al., 2012)	Originally from Dr. Bruce Torbett
Phi-Eco (retroviral helper)	Gift (Kira Gritsman)	N/A
pMD2.G (lentiviral helper)	Addgene	12259
Chemicals, peptides, and recombinant proteins		
Murine recombinant IL-3	GEMINI	300-324P
Murine recombinant IL-6	GEMINI	300-327P
Murine recombinant Flt3-Ligand	GEMINI	300-306P

(Continued on next page)

Continued

REAGENT or RESOURCE	SOURCE	IDENTIFIER
Murine recombinant SCF	GEMINI	300-348P
Murine recombinant TPO	GEMINI	300-351P
ALRN-6924	Aileron Therapeutics	N/A
BC2059	Targetmol	T5642
BrdU (5-Bromo-2'-deoxyuridin)	Sigma-Aldrich	19160
MG132 , Ready Made Solution	Sigma-Aldrich	M7449
PNU75654	Selleckchem	S8429
Puromycin dihydrochloride	Sigma-Aldrich	P8833
WNT974 (LGK974)	InvivoChem	V1353

Critical commercial assays

CD117 (cKit) MicroBeads, mouse	Miltenyi Biotec	130-091-224
CellTiter-Blue Cell Viability Assay	Promega	G8081
cOmplete Protease Inhibitor Cocktail (IP/WB)	Millipore Sigma	11697498001
Dynabeads Untouched Mouse T cells (negative depletion)	Thermo Fisher Scientific	11413D
FITC BrdU Flow Kit	BD Pharmingen	51-2354AK
iScript cDNA Synthesis Kit	BIO-RAD	1708890
Mouse methylcellulose complete media	R&D systems	HSC007
Nucleospin Plasmid (cloning)	Takara Bio	740588
Pierce Anti-DYKDDDDK(FLAG) magnetic beads	Thermo Scientific	A36797
Pierce Anti-HA magnetic beads	Thermo Scientific	88836
Phosphatase inhibitor cocktail 2 (IP/WB)	Sigma-Aldrich	P5726
Phusion High-Fidelity DNA Polymerase (cloning)	Thermo Scientific	F530
Phusion Site-Directed Mutagenesis Kit (cloning)	Thermo Scientific	F541
Polybrene (virus transduction)	Santa Cruz Biotechnology	Sc-134220
Power SYBR Green PCR Mster Mix	Applied biosystems	4367659
Primocin	InvivoGen	ant-pm
QIAquick Gel Extraction Kit (cloning)	QIAGEN	28704
QIAquick PCR Purification Kit (cloning)	QIAGEN	28106
RetroNectin (virus transduction)	Takara Bio	T100
RNeasy Micro Kit (RNA extraction)	QIAGEN	74004
StemSpan SFEM	STEMCELLS	09600

Deposited data

All RNA sequencing data	This paper	GSE164838
Gene expression data of MDS cohort	(Bhagat et al., 2017)	GSE19429

Experimental models: cell lines

Human: HEK293T cell line	ATCC	Cat# CRL-3216; RRID: CVCL_0063
Human: HL-60	ATCC	Cat# CCL-240 RRID: CVCL_0002
Human: OCI-AML3	Leibniz Institute	Cat# ACC-582 RRID: CVCL_1844
Mouse: 32D (clone3)	ATCC	Cat# CRL-11346 RRID: CVCL_0119

Experimental models: organisms/strains

Mouse: B6(Cg)-Tet2 ^{tm1.2Rao}	Jackson	023359
--	---------	--------

(Continued on next page)

Continued		
REAGENT or RESOURCE	SOURCE	IDENTIFIER
Mouse: B6.129- <i>Flt3^{tm1Dgg}/J</i> (<i>Flt3^{WT/ITD}</i>)	Jackson (Lee et al., 2007)	011112
Mouse: B6.129S2- <i>Trp53^{tm1Tyj}/J</i> (<i>Trp53^{-/-}</i>)	Jackson	002101
Mouse: B6.SJL-Ptprca Pepcb/BoyJ (Ly45.1)	Jackson	002014
Mouse: C57BL/6J	Jackson	000664
Mouse: <i>Mdmx</i> -Tg (Tg-15)	(Xiong et al., 2010)	N/A
Mouse: NOD.Cg- <i>Prkdc^{scid}Il2rg^{tm1Wjl}/SzJ</i> (NSG)	Jackson	005557
Mouse: <i>PU.1</i> URE ^{-/-}	(Rosenbauer et al., 2004)	N/A
Oligonucleotides		
See Table S5		
Recombinant DNA		
pCMV3.(Human)MDM4-Flag	Sino Biological	HG15395-CF
FUW.(Human) <i>MDMX</i> .IRES.Puro lentiviral vector	This paper	N/A
FUW.(Mouse) <i>Mdmx</i> .IRES.Puro lentiviral vector	This Paper	N/A
MSCV. <i>NRAS</i> -G12D.IRES.GFP retroviral vector	(Parikh et al., 2007)	N/A
MSCV.(Mouse) <i>Csnk1a1</i> .IRES.GFP retroviral vector	(Jaras et al., 2014)	N/A
pCAD.(Mouse) <i>Mdmx</i> .IRES.GFP lentiviral vector	This paper	N/A
pGFP-C-shLenti control shRNA	Origene	TR30021
pGFP-C-shLenti shRNA for <i>Ctnnb1</i> -A	Origene	TL500280A
pGFP-C-shLenti shRNA for <i>Ctnnb1</i> -B	Origene	TL500280B
Software and algorithms		
CompuSyn ver.1.0	Compusyn Inc, (Chou, 2006)	http://www.combosyn.com/
DESeq2	(Love et al., 2014)	http://bioconductor.org/packages/release/bioc/html/DESeq2.html
FastQC	Babraham Bioinformatics	https://www.bioinformatics.babraham.ac.uk/projects/fastqc/
FlowJo_10.6.1_CL	FlowJo	https://www.flowjo.com/
GSEA 4.0.2	Broad institute	https://software.broadinstitute.org/gsea/index.jsp
GraphPad Prism 8	GraphPad	https://www.graphpad.com/scientific-software/prism/
IPA v01.13	Qiagen	https://www.qiagenbioinformatics.com/products/ingenuity-pathway-analysis
Volocity Quantitation	Quorum Technologies	https://quorumtechnologies.com/volocity/volocity/quantitation
R v3.6.0	R Core Team	www.r-project.org
Salmon v0.11.3	(Patro et al., 2017)	https://salmon.readthedocs.io/en/latest/salmon.html

RESOURCE AVAILABILITY

Lead contact

Further information and requestst for resources and reagent should be directed to and will be fulfilled by the Lead Contact, Ulrich Steidl (Ulrich.steidl@einsteinmed.org).

Materials availability

Plasmids are detailed in the [Key resources table](#) and available upon request. The sequence of oligos are detailed in [Table S4](#). Mouse models used in this study are detailed in the [Key resources table](#) and available upon request.

Data and code availability

RNA sequencing data sets of murine HSC/pre-LSC were deposited (GSE164838). Publicly available gene expression data sets of a large MDS cohort (GSE19429) were used for the analysis.

EXPERIMENTAL MODEL AND SUBJECT DETAILS

Cell lines

Human HL-60 cells were cultured in IMDM medium supplemented with 20% Fetal Bovine Serum (FBS) and 1% penicillin streptomycin. FUW-*MDMX*-IRES-Puro or empty vector (FUW-IRES-Puro) was transduced into HL-60 as previously described ([Ito et al., 2019](#)) to generate MDMX-overexpressing HL-60 and control. Human OCI-AML3 cells were cultured in α MEM medium supplemented with 20% FBS and 1% penicillin streptomycin. Mouse 32D leukemia cells were cultured in IMDM medium supplemented with 10% Fetal Bovine Serum (FBS), 10% WEHI conditioned media (including murine IL3) and 1% penicillin streptomycin. FUW-*Mdmx*-IRES-Puro, pCAD-*Mdmx*-IRES-GFP, MSCV-Csnk1a1-IRES-GFP or empty vectors were transduced into 32D as previously described ([Kawahara et al., 2012](#)) to generate MDMX and/or CSNK1A1 (CK1 α) overexpressing 32D and controls. FUW-*MDMX*-IRES-Puro or empty vectors were transduced into HL-60 to generate MDMX overexpressed HL-60.

Animal studies

All animal experiments were performed in compliance with institutional guidelines and approved by the Animal Institute Committee of the Albert Einstein College of Medicine (#00001099). The origin of murine models used in the study are detailed in the [Key resources table](#). For competitive transplantation assays and *Nras*-G12D transplantation assays, *Mdmx*-Tg were backcrossed to C57BL/6J at least 8 generations. For other analyses, mice were used in Sv129 and C57BL/6J mixed background. *Mdmx*-Tg were bred with *PU.1* URE^{+/-} or *Flt3*^{ITD/ITD}, for generation of generated URE^{-/-}; *Mdmx*-Tg and *Flt3*^{WT/ITD}; *Mdmx*-Tg animals with controls. 10 to 14-week-old male mice were used for the experiments otherwise specified.

Clinical samples

Bone marrow samples from patients with MDS were obtained after written informed consent, from Montefiore Medical Center / Albert Einstein Cancer Center (IRB# 11-02-060E).

METHOD DETAILS

Analyses of murine models

Peripheral blood was counted using FORCYTE or Genesis Hematology System (Oxford Science) instruments. Spleen and thymus were weighed, and cells were dissociated on 70 μ m filters. BM cells were collected by crushing bones (tibia, femur, iliac, sternum and vertebrae). 1×10^5 cells of spleen and BM were used for cyto-spin, and cells were stained by standard Wright-Giemsa staining. For further analysis of nuclear cells, red blood cells were lysed with lysis buffer (150mM NH₄Cl, 1mM KHCO₃ and 0.1mM EDTA).

Flow cytometry (FCM)

1×10^6 nuclear cells of spleen and thymus or 5×10^6 nuclear cells of BM were stained (see [Table S4](#)) for FCM analysis using FACS Aria2 (BD Biosciences). Definition of HSC/HSPC fractions was described previously ([Kondo et al., 1997](#); [Mayle et al., 2013](#); [Pietras et al., 2015](#)). Thymus cells were analyzed as previously described ([Tremblay et al., 2010](#)).

In vivo BrdU assays

BrdU assay was performed as previously described with minor modifications ([Liu et al., 2009](#)). Briefly, BrdU was administered by mixing into drinking water (1mg/ml). After 48 hours, mice were sacrificed and BM cells were stained by biotin-conjugated lineage markers (see [Table S5](#)). 2.5×10^5 Lineage negative cells were selected by Magnetic-activated cell sorting system (MACS; Miltenyi Biotec), and stained for additional FCM antibodies (see [Table S5](#)). Cells were fixed, permeabilized and stained with FITC-conjugated anti-BrdU antibody and 7AAD (BD Pharmingen), and analyzed using a FACS Aria II instrument.

In vitro colony forming assays

Bulk BM cells or sorted HSPCs/HSCs/pre-LSCs were spread in 1mL cytokine-containing methylcellulose media (HSC007 for mouse, HSC003 for human, R&D systems), and plated in 35mm culture dish. For murine cells, colonies were counted and replated after 7 days.

Competitive transplantation assays

1×10^6 donor cells (Ly45.2) and 1×10^6 WT competitors (Ly45.1/2 double positive) were transplanted into lethally irradiated (12Gy split dose) recipients (Ly45.1). 20 μ l of peripheral blood was collected monthly, lysed with lysis buffer (150mM NH₄Cl, 1mM KHCO₃ and

0.1mM EDTA) and stained (see Table S5) to measure ratio of Ly45.2 using a FACS Aria II. Also, p53^{-/-} and p53^{-/-};Mdmx-Tg recipients were sacrificed 4 months after transplantation, and BM cells were collected. 5x10⁶ cells were stained (see Table S4) to measure the ratio of CD45.2 using a FACS Aria II instrument. For homing assay, ratio of Ly45.2 in BM was measured at 1 week from transplantation.

Transplantation assay of preleukemic/leukemic BM cells

1x10⁶ BM cells/recipient from preleukemic/leukemic URE^{-/-} or URE^{-/-};Mdmx-Tg mice were transplanted into sublethally (2Gy) irradiated NSG mice. 1x10⁵ sorted GFP⁺ BM cells from *Nras*-G12D leukemic recipients were serially transplanted into lethally (12Gy split dose) irradiated recipients (Ly45.1).

Spectral karyotyping (SKY)

Lineage-negative cKit-positive BM cells were sorted from *Flt3*^{WT/ITD};Mdmx-Tg AML mice, and cultured overnight. Cells were stained and analyzed for mitotic phase cells as previously described (Montagna et al., 2003; Padilla-Nash et al., 2006).

RNA sequencing (RNA-seq)

1x10⁴ HSCs (WT and Mdmx-Tg) or pre-LSCs (URE^{-/-} and URE^{-/-};Mdmx-Tg) were sorted using a FACS Aria II instrument (see Table S4). Total RNA was isolated using RNeasy Micro Kit. Total RNA was subjected to mRNA enrichment, fragmentation, cDNA synthesis, adapter ligation, and PCR amplification for library construction, with incorporation of the DNA nanoball technology as previously described (Zhu et al., 2018). RNA-seq was performed by BGI Americas using the BGISEQ-500 platform, paired-end 100-bp read length (Xu et al., 2019). Cleaned and trimmed reads were analyzed by FastQC for base sequence quality, GC content, N content, and sequence duplication levels. Sequencing reads passing quality control criteria were aligned to the Mus Musculus (mm10/GRCm38) transcriptome and quantified using Salmon (Patro et al., 2017). Raw counts were normalized and analyzed for differential expression in R using the Bioconductor package DESeq2 (Love et al., 2014). For GSEA analysis, pre-ranked gene lists were generated using the negative logarithm of the adjusted p-value multiplied by the sign of the fold change for each gene (Equation 1), and input into GSEA Preranked to calculate the enrichment score for each gene set (Subramanian et al., 2005). Pre-ranked gene lists were queried against standard MSigDB gene sets, including hallmark and c1-7 curated gene sets, as well as selected p53 and β-catenin gene lists. In parallel, DESeq2 results were input into IPA for further pathway enrichment analysis (<https://www.qiagenbioinformatics.com/products/ingenuitypathway-analysis>).

$$\text{Score} = -\log(\text{pval}_{\text{adj}}) \times \text{sign}(\text{fold-change}) \quad (\text{Equation 1})$$

Immunofluorescence (IF) staining

Sorted primary Flk2- LSK cells were plated on retronectin coated coverslips and incubated at 4 degree for 30 min prior to fixation. After microscopic confirmation of cell attachment, cells were fixed with 3.2% PFA in PBS for 10 min at room temperature followed by permeabilization in 0.2% Triton X-100 in PBS for 10 min at room temperature. Blocking was done in blocking buffer (1% BSA/0.1% TritonX-100/1XPBS) for 30 min at room temperature. Cells were then incubated overnight at 4 degrees with 1:500 dilution of rabbit anti-β-Catenin (Cell Signaling) in blocking buffer. Cells were washed 3 times in PBS and incubated for 2 hours at room temperature in 1:1000 dilution of AF488-conjugated goat anti-rabbit IgG (abcam) in blocking buffer. Slides were then washed 3 times in PBS and mounted using ProLong Diamond Antifade Mountant with DAPI (Invitrogen, P36962). Cells were imaged on a Leica SP8 Upright Confocal Microscope (Leica, with 63X objective). Images were processed and analyzed using Volocity® Quantitation software.

Western blotting (WB)

Whole cell extracts were prepared using lysis buffer (150mM NaCl, 50mM Tris-Cl, 5mM EDTA, 1% NP-40, 1% Phosphatase inhibitor cocktail, 1X Protease Inhibitor Cocktail, 1mM PMSF, 10% Glycerol). SDS-PAGE was performed with equal amounts of protein per sample and transferred to PVDF membranes for further immunoblotting using primary antibodies (1:5000 for Actin, 1:2000 for LaminB and β-Tublin, and 1:1000 for others; See Key resources table) followed by HRP-conjugated secondary antibodies (1:5000; See Key resources table). Imaging of western blots was performed using chemiluminescent ECL substrate on a LI-COR Odyssey Fc imager.

Immunoprecipitation and mass-spectrometry (IP and LC-MS/MS)

For MDMX interactome screening, equal numbers of cells were lysed in mild lysis buffer (1XPBS, 1%NP-40, 0.1% TritonX-100, 1% Phosphatase inhibitor cocktail, 1X Protease Inhibitor Cocktail, 1mM PMSF) followed by IP with HA-conjugated magnetic Dynabeads and eluates were submitted for mass-spectrometry analysis to MS Bioworks. Briefly, cells were incubated in lysis buffer with intermittent vortexing on ice for 45 minutes. The lysates were centrifuged at 13,000g for 15 minutes and supernatant was diluted 5 times with 1X PBS to effectively reduce the concentration of NP-40 to 0.2%. Immunoprecipitation was performed using anti-HA or anti-FLAG magnetic beads and bound proteins were eluted using 0.1M glycine pH2.0. Eluate was neutralized by neutralization buffer (1M Tris, pH8.5). Mass spectrometry data was analyzed using Scaffold Proteome software and significantly detected proteins were shortlisted for further analysis.

Subcellular fractionation

Subcellular fractionation was performed using the REAP method as described previously (Nabbi and Riabowol, 2015). Briefly, equal numbers of cells per condition were resuspended in low NP-40 buffer (0.1%NP-40 in 1XPBS, 1mM PMSF, 1% Phosphatase inhibitor cocktail, 1X Protease Inhibitor Cocktail) and rotated at 4°C for 10 minutes followed by centrifugation at 10,000g for 60 seconds. Obtained supernatant was designated as cytoplasmic extract. Pellets were washed with PBS twice to remove residual cytoplasmic contaminants and further sonicated for 5 minutes in buffer (1%NP-40 and 0.1% TritonX-100 in 1XPBS, 1mM PMSF, 1% Phosphatase inhibitor cocktail, 1X Protease Inhibitor Cocktail). Sonicated nuclear pellets were centrifuged at 13,000g for 15 minutes and supernatant was transferred and labelled as nuclear extract.

Quantitative reverse transcriptase-polymerase chain reaction (qRT-PCR)

RNA was isolated from 5.0×10^5 32D or HL-60 cells using RNeasy Micro Kit. Reverse transcriptase reaction (RT) was performed with 1 μ g of total RNA using the iScript cDNA Synthesize Kit followed by polymerase chain reaction (qPCR) using Power SYBR Green Master Mix on a ViiA7 Real Time PCR System (ThermoFisher). Expression levels were normalized by GAPDH. Primer sequences are available in Table S5.

Cell viability assay (IC50)

For primary pre-LSC model, lineage-negative cKit-positive cells from BM of preleukemic URE^{-/-}; *Mdmx*-Tg mice were sorted using a FACS-Aria II instrument (BD Biosciences). 2×10^4 Cells were cultured in 100 μ l of StemSpan SFEM supplemented with 5% FBS, 1% glutamine, 100 μ g/ml Primocin, 50ng/ml recombinant mouse SCF, TPO, FLT3-L, IL3 and IL6 with various concentrations of PNU74654 and/or ALRN-6924 for 16 hours. For leukemia model, 1×10^4 OCI-AML3 cells were cultured as described above (see “Cell Lines”) with various concentrations of drugs for 24 hours. All cells were cultured in 96-well flat bottom culture dishes by triplicate for each condition. After culture, 20 μ l of CellTiter-Blue Viability Assay was added, and resazurin fluorescence (560_{EX}/590_{EM}) was measured using an FLUOstar Omega instrument (BMG Labtech). IC50 and combination-index (CI) were calculated by CompuSym software (Chou, 2006).

Plasmid construction

For cloning of human MDMX, we purchased pCMV3-*MDMX*(*MDMX*)-Flag and the insert was amplified with primers harboring BamH1 sites at 5'-UTR and 3'UTR (see Table S5). The amplified DNA was cloned into the FUW-IRES-Puro (Ito et al., 2019) lentiviral vector using the BamH1 site. For murine *Mdmx*, we amplified the insert of a murine *Mdmx* target vector (Xiong et al., 2010) using primers harboring EcoR1 sites at 5'-UTR and 3'UTR (see Table S5). The amplified DNA was sequenced for validation and cloned into pCAD-IRES-GFP lentiviral vector (Kawahara et al., 2012), and an HA-tag was added using Phusion Site-Directed Mutagenesis Kit. In addition, HA-tagged murine *Mdmx* was cloned into the FUW-IRES-Puro lentiviral vector using EcoR1 site. Other plasmids are detailed in the Key resources table.

Virus production and transduction

15 μ g Lentiviral/retroviral vectors were transfected to 293T cells spread in 100mm culture dish with helpers (7.5 μ g PAX2 and 2.5 μ g pMD2.G for lentivirus, 7.5 μ g Phi-Eco for retrovirus) using Polyethyleneimine as previously described (Reed et al., 2006). Virus-containing supernatant was collected and filtered at 48 hours and 72 hours from transfection. For cell lines, virus was transduced into cells by centrifuging at 1000g, 37 Celsius, 1 hour with 10 μ g/ml polybrene. For primary cells, virus was attached on retronectin-coated 24 well dishes by centrifuging 1000g, 37 Celsius, 2 hours and cells were centrifuged at 1000g on virus-attached dish for 1 hour.

QUANTIFICATION AND STATISTICAL ANALYSIS

All statistical analyses except for Figure 8 were performed by GraphPad PRISM 8. Student t-test or Wilcoxon-test were used for the comparisons of the means of two groups. The Tukey HSD-test was used for the comparisons of the means of more than two groups. The Log-rank test was used for the survival curve analyses. N represents biological replicates in cell culture experiments and the number of mice in animal studies. For Figure 8, R fundamentals and package “cmprsk” were used.